Separation and Purification Technology 354 (2025) 129355

Contents lists available at ScienceDirect

Separation and Purification Technology

journal homepage: www.elsevier.com/locate/seppur

Production of high-grade antimony oxide from smelter slag via leaching and hydrolysis process

Ahmedaljaali Ibrahim Idrees Ibrahim [a], Muhammed Aboelgamel [a], Kartal Kaan Soylu [a], Soner Top [b,*], Sait Kursunoglu [c,*], Mahmut Altiner [a,*]

[a] Division of Mineral Processing, Department of Mining Engineering, Cukurova University, 01330 Adana, Turkey
[b] Department of Engineering Science, Abdullah Gul University, 38080 Kayseri, Turkey
[c] Department of Petroleum and Natural Gas Engineering, Batman University, 72100 Batman, Turkey

ARTICLE INFO

Keywords:
Antimony
Smelter slag
HCl leaching
Hydrolysis
Rare earth elements

ABSTRACT

This study aimed to investigate the recovery of antimony (Sb) from slag generated in an antimony smelting plant using leaching followed by hydrolysis processes. The leaching behaviors of rare earth elements (REEs) were also examined. The physicochemical properties of the slag were determined using various analytical techniques. The slag (4.12 % Sb) was mainly composed of quartz and minor minerals, including microline, magnetite, hedenbergite, and stibiconite. The Sb types in the slag determined by XPS were found to be in the oxide form. The concentrations of REEs (La, Y, Ce, and Nd) in the slag were 169.21 g/t. Preliminary leaching experiment results indicate that (i) HCl was selected rather than other acids due to its high extraction ability on the Sb from the slag, (ii) a sample with a d_{50} of < 25 μm should be used, (iii) the slurry should be mixed at 300 rpm. In the following leaching tests, the effects of leaching parameters (HCl acid concentration, amount of tartaric acid, solid-to-liquid ratio, reaction temperature, and time) on the extraction rates of Sb, impurities, and REEs were investigated. At the best leaching conditions (HCl: 8 M, amount of tartaric acid: 1 g/L, stirring speed: 300 rpm, reaction temperature: 75 °C, and time: 180 min), the extraction rates of Sb from the slag were determined to be 91.19 %, but the extraction rates of REEs were measured to be $\leq$ 50 %. The activation energy (Ea) for Sb leaching was found to be 46.75 kJ/mol, indicating that the reaction was governed by the chemically controlled mechanism. In particular, it was understood from the additional experimental results that the leaching procedure should be carried out for 20 h to extract La with an extraction rate of $>$ 90 %. However, the extraction rate of Sb was negligible in extended times. It was determined that using tartaric acid positively affected La's leaching mechanism, and the required leaching time for La decreased to 180 min from 20 h with the increase of tartaric acid from 1 g/L to 6 g/L. Hydrolysis tests were conducted using the Taguchi approach (L32, 2^1 4^3). The effects of the alkaline type (NH_4OH and NaOH), stirring speed (100, 200, 300, and 400 rpm), temperature (50, 60, 70, and 80 °C), and pH (1.5, 2, 2.5, and 3) on the precipitation of Sb from the PLS were investigated. NH_4OH was suggested for use in the hydrolysis test to obtain precipitates with higher purities. The product obtained under the optimal conditions comprised 81.43 % Sb, 16.23 % O, and 2.34 % Fe. The product was identified as antimony oxide by XRD.

1. Introduction

Antimony (Sb) is a brittle, silver-white, shiny, and important metal with a specific gravity of 6.68 g/cm^3 and a melting point of 630 °C, which is widely used in modern industrialized societies today. Sb metal breaks too easily to be used on its own, but it gives strength, hardness, and resistance to corrosion to alloys [1]. Sb is rarely found in its native form due to its strong affinities with other elements, including sulfur, copper, lead, gold, arsenic, and silver [2]. There are more than 100 antimony-bearing minerals present in the nature, but the most common one is stibnite (Sb_2S_3) mineral.

Sb with superior properties has many uses in the industry, such as in the hardening of metals, protection against corrosion and fire, paper, plastic, paint, and photovoltaics. For instance, lead-acid accumulators

* Corresponding authors.
E-mail addresses: soner.top@agu.edu.tr (S. Top), sait.kursunoglu@batman.edu.tr (S. Kursunoglu), maltiner@cu.edu.tr (M. Altiner).

https://doi.org/10.1016/j.seppur.2024.129355
Received 2 July 2024; Received in revised form 21 August 2024; Accepted 23 August 2024
Available online 24 August 2024

Table 1
The chemical composition of the slag.

Element	Al	Ca	Fe	K	Mg	Mn	Na
Amount (wt.%)	2.10	1.32	2.12	0.55	0.51	0.05	<0.05
Element	Cu	Sb	Ni	P	Si	Ti	Cr
Amount (wt.%)	0.03	4.13	0.04	<0.01	33.39	0.09	0.03
Element	S	Loss on ignition: 2.60 wt%					
Amount (wt.%)	0.51						

Table 2
The concentration of REEs and other elements in the slag.

Element	Ce	Dy	Er	Eu	Gd	Ho	La
Amount (g/t)	31.11	3.91	1.10	0.44	4.46	1.24	78.52
Element	Lu	Nd	Tb	Th	Tm	U	Co
Amount (g/t)	0.45	33.78	0.96	2.43	0.34	24.30	11.65
Element	Y	Yb	Lu	Pt	As	Cd	Pb
Amount (g/t)	25.80	0.87	0.11	5.32	441.00	13.00	93.80
Element	Sc	Sm	Pr	Rb	Li	Sr	V
Amount	3.41	2.56	6.17	84.55	39.60	47.60	33.70
Element	W	Zn	Zr	Ni	Ba	Be	Bi
Amount (g/t)	0.16	942.00	23.50	348.00	43.50	1.50	0.03
Element	Cr	Ga	Ge	Mo	Au	Ag	
Amount (g/t)	356.00	6.15	0.14	11.95	3.70	23.70	

(the kind commonly used in automobiles) contain lead–alloyed antimony by 4–6 %, and antimony's resistance to corrosion is the reason why the so-called "lead" battery terminals are made of lead-antimony alloy. Very high-purity antimony metal (99.99 % + pure) is used by the semiconductor industry as the main component for infrared detectors, diodes, and other devices and applications in silicon sheets in the form of compounds such as InSb, GaSb, and SbTe [3]. Moreover, Sb in the form of antimony trioxide (Sb_2O_3) is a widely used flame retardant across many different industries such as; adhesives (to decrease the fire risk), paints (to prevent flames and smoke from the layer during a fire), paper (to reduce the fire risk and allow the paper products to withstand fire for long periods), plastic (to increase the durability of the product in case of fire), rubber and textile floor coverings (as a fire retardant additive). The main markets for flame-retardants include electronics, plastics, and fabrics used in the construction of children's clothing, airplane and automobile seat covers, and bedding. In the semiconductor industry, silicon wafers containing very high-purity antimony metal are used to create infrared detectors, diodes, and other electronic components. Sb_2O_3 is also evaluated in additional applications such as glass production, alloys, brake pads, lithium–sodium batteries, and battery production [4–7].

Sb_2O_3 was also added as a clarifying agent in solar glasses during the production of transparent photovoltaic panels. It is well known that Sb_2O_3 significantly enhances the properties of solar glass, making it an essential material for sustainable energy production. The demand for Sb_2O_3 is expected to increase due to the rapid expansion of its use in the photovoltaic industry. The Sb_2O_3 thin films doped with various elements (Ag, F, Ni, Cu, Er, and Co) were prepared through different techniques, including spray pyrohydrolysis [8] and thermal evaporation [9]. Among them, previous researchers have suggested to use F-doped Sb_2O_3 films that can be utilized in many optoelectronic and photovoltaic applications [8].

Table 3
The parameters investigated in the leaching test.

Parameters	Value
Particle size (d_{50})	<25 μm
Stirring speed (rpm)	300
Acid concentration (M)	1, 2, 3, 4, 5, 6, 7, 8, and 9
Amount of tartaric acid (g/L)	0, 1, 3, 5, and 6
Solid-to-liquid ratio (g/mL)	1/8, 1/10, 1/12, and 1/15
Time (min)	45, 75, 90, 180, 240, 360, 480, 600, 900, and 1200
Temperature (°C)	Room temperature, 40, 60, and 75

Table 4
Different chemical kinetic models and equations used in this study.

Model	Equation
Inner diffusion-controlled model	$1-2/3\alpha+(1-\alpha)^{2/3}=k\times t$
Liquid boundary layer diffusion controlled model (Jander equation)	$1-(1-\alpha)^{2/3}=k\times t$
Chemical reaction controlled model	$1-(1-\alpha)^{\frac{1}{3}}=k\times t$
Both chemical and diffusion controlled	$1-2(1-\alpha)^{\frac{1}{3}}+(1-\alpha)^{2/3}=k\times t$

There are many reports published in recent years by different countries around the world (Australia, South Korea, Canada, The United States of America, and Japan), country communities (European Union, EU), research institutions (British Geological Survey), and the World Bank [10]. When these reports are examined, it is seen that antimony (Sb) metal is considered as one of the "most important critical raw materials" in terms of supply risk and economic value in seven of the eight lists. Moreover, antimony is not only present in the 2023 report also have been in the critical raw materials reports published in 2011, 2014, 2017, and 2023 [11]. Although China is the largest supplier of antimony, the report published by the EU (2023) indicates that Turkey is the major supplier of antimony with a rate of 63 % for EU countries, whereas the rest of the antimony supply was provided by Bolivia (26 %) and China (6 %).

It is seen that antimony mine production in China accounts for 49 % of global antimony mine production. However, Zhong et al. [12] predicted that known antimony reserves will be depleted by 2050 due to the rates of ore production. Anderson [13] (2019) indicated that the demand for Sb in lead-acid batteries will decrease, but the use of Sb in flame-retardants will increase in the plastics industry. Therefore, it is inevitable that metallurgical slags will evaluated as secondary Sb resources, except for primary ores and end-of-life products (lead-acid batteries). Also, the use of these slags as raw Sb sources decreases the potential pollution of the environment [14]. Although there are many studies on the production of Sb from an antimony ore in the literature, studies focused on the recovery of Sb remaining in the slag after the pyrometallurgical process by using hydrometallurgical methods are limited. These studies focus on the recovery of Sb found in anode slime resulting from pyrometallurgical processes involving metals such as lead, copper, and tin [15–19].

The production of Sb from primary ores is a well-known process and is described in detail in previous studies [20,21]. However, the recovery of Sb from end-of-life products and metallurgical slag should be investigated in detail to gain knowledge of Sb recovery. Currently, there are many studies carried out using pyrometallurgical or hydrometallurgical processes on the recovery of Sb from different industrial wastes lead-acid battery [15,22,23], metal oxide varistors [24,25], smelter slag [4], arsenic filter cake [26], Sb containing concentrates (copper concentrate [27,28]), copper electro-refining stream [29], antimony-rich oxidizing slag [30], Sb-bearing dust [12], etc. Dupont et al. [31]

Table 5
Hydrolysis experiments parameters with their levels.

Parameters	Level
Alkaline types	NH_4OH and NaOH
Stirring speed (rpm)	100, 200, 300, and 400
Temperature (°C)	50, 60, 70, and 80
pH	1.5, 2, 2.5, and 3

Table 6
The experimental conditions in the hydrolysis test.

Exp. No	Alkaline type	Stirring speed	Temperature	pH	Exp. No	Alkaline type	Stirring speed	Temperature	pH
1	NH_4OH	100	50	1.5	17	NaOH	100	50	3
2	NH_4OH	100	60	2	18	NaOH	100	60	2.5
3	NH_4OH	100	70	2.5	19	NaOH	100	70	2
4	NH_4OH	100	80	3	20	NaOH	100	80	1.5
5	NH_4OH	200	50	1.5	21	NaOH	200	50	3
6	NH_4OH	200	60	2	22	NaOH	200	60	2.5
7	NH_4OH	200	70	2.5	23	NaOH	200	70	2
8	NH_4OH	200	80	3	24	NaOH	200	80	1.5
9	NH_4OH	300	50	2	25	NaOH	300	50	2.5
10	NH_4OH	300	60	1.5	26	NaOH	300	60	3
11	NH_4OH	300	70	3	27	NaOH	300	70	1.5
12	NH_4OH	300	80	2.5	28	NaOH	300	80	2
13	NH_4OH	400	50	2	29	NaOH	400	50	2.5
14	NH_4OH	400	60	1.5	30	NaOH	400	60	3
15	NH_4OH	400	70	3	31	NaOH	400	70	1.5
16	NH_4OH	400	80	2.5	32	NaOH	400	80	2

Table 7
The experimental conditions of additional hydrolysis test.

Exp. No	Alkaline type	Stirring speed (rpm)	Temperature (°C)	pH
HE-1	NH_4OH	100	50	1.5
HE-2	NH_4OH	100	50	1.25
HE-3	NH_4OH	100	50	1.00
HE-4	NaOH	100	50	1.5
HE-5	NaOH	100	50	1.25
HE-6	NaOH	100	50	1.00

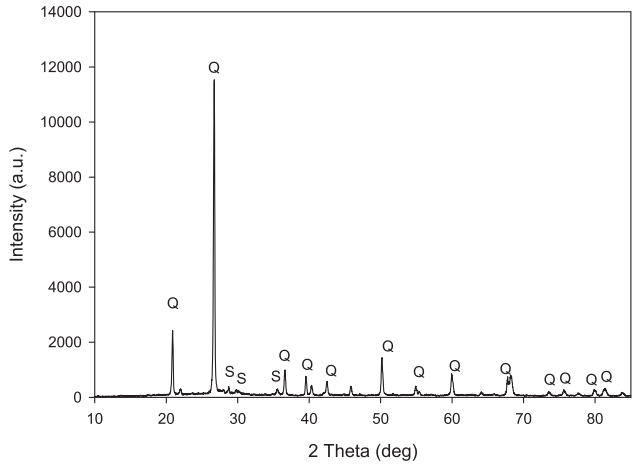

Fig. 1. XRD pattern of the slag used in this study (Q: Quartz, S: Stibiconite).

reviewed in detail the recovery of Sb from end-of-life and industrial process residues. In another work, the trends, applications, and strategies in the Sb recovery were systematically reviewed by researchers [32]. Three options, including electrodeposition, hydrolysis, and cementation, can be conducted on the recovery of antimony from the pregnant leachate solution (PLS) [33].

It is possible to process complex antimony ores with this method. Based on the mineralogical composition of raw material, acid or alkaline leaching can be applied. For example, the selective dissolution of Sb with an extraction rate of 96.64 % from a stibnite ore was possible in the alkaline (Na_2S – NaOH) medium [34,35]. The recovery of Sb and Bi from tin anode slime was investigated using soda roasting followed by alkaline leaching processes [16]. However, it was stated that the leaching behavior of Sb from Sb-bearing ores was investigated based on pH-dependent release characteristics [36]. Also, different leaching agents, including $FeCl_3$ [35], HCl with ozone [37], and HCl-NaCl [38], can be used to provide an acidic medium to extract Sb from different raw materials. In another study, Sb with an extraction rate of 98.53 % from ore was dissolved under the following conditions: a temperature of 50 °C, an 8:1 of liquid-to-solid ratio, and a time of 1 h. There was no need to use oxidants for the leaching of Sb [33]. However, the addition of tartaric acid prevents the precipitation of Sb dissolved during the HCl leaching [39,40]. NaCl was further used to prevent Sb hydrolysis. Previous research suggested the use of ultrasonic treatment during the leaching. The required reaction time for the leaching of Sb with high extraction rates by conducting ultrasonic power was three times lower compared to that of the regular leaching procedure [30]. Slurry electrolysis (a combination of leaching, purification, and electrolysis) was recommended to extract Sb from high As and Au-containing stibnite ore [41]. In another work, a potential-controlled chlorination leaching process was suggested to increase the extraction of Sb. The solution potential increased from 260 to 450 mV with the addition of Cl_2 and Sb, which was dissolved with an extraction rate of > 99 % [42]. Sudova et al. [43] suggested the use of deep eutectic solvents (a mixture of choline chloride and ethylene glycol) in the presence of iodine as an oxidant for the extraction of Sb from mining residues and all of Sb was dissolved at a temperature of 100 °C for 4 h.

Previous researchers stated that the presence of Fe ions in the solution may create problems in terms of the precipitate's purity, as the precipitation rate of Sb and Fe reached 99 % with the addition of NH_4OH. The separation mechanism of Sb from an Sb-Fe mixed solution was systemically investigated by the hydrolysis technique [44]. Hashimoto et al. [45] determined the chemical equilibrium conditions of the Sb(III)-HCl-H_2O system and subsequently obtained various morphological properties of Sb compounds by precipitation with the addition of NaOH. Sb_2O_3 particles [46] were prepared with the addition of NH_4OH into $SbCl_3$ solution in the pH range of 8.5–9. Some researchers have recommended for use of water to conduct the hydrolysis process for Sb, but their aging period was too long and the required aging time to obtain Sb precipitate was found to be 7 days with a recovery of 97 % [47]. Additionally, there is a study focusing on the characterization of crude products containing high levels of As and Pb obtained from an antimony smelting plant, which contains about 82–82.5 % Sb [48]. The removal of As in the crude product is achieved through HNO_3 leaching [49]. Unlike previous studies, the use of a different residue source in this study, especially with a material composition different from the studies in the literature in terms of chemical content, is expected to positively contribute to the uniqueness of the study. It was planned to develop a process for Sb and Rare Earth Elements (REEs) recovery from a smelter slag generated during the processing of antimony ore. Preliminary studies indicated that the slag used in this study could be further evaluated as raw materials for REEs due to its content. Therefore, the work planned to be carried out in this study consists of four (4) work stages.

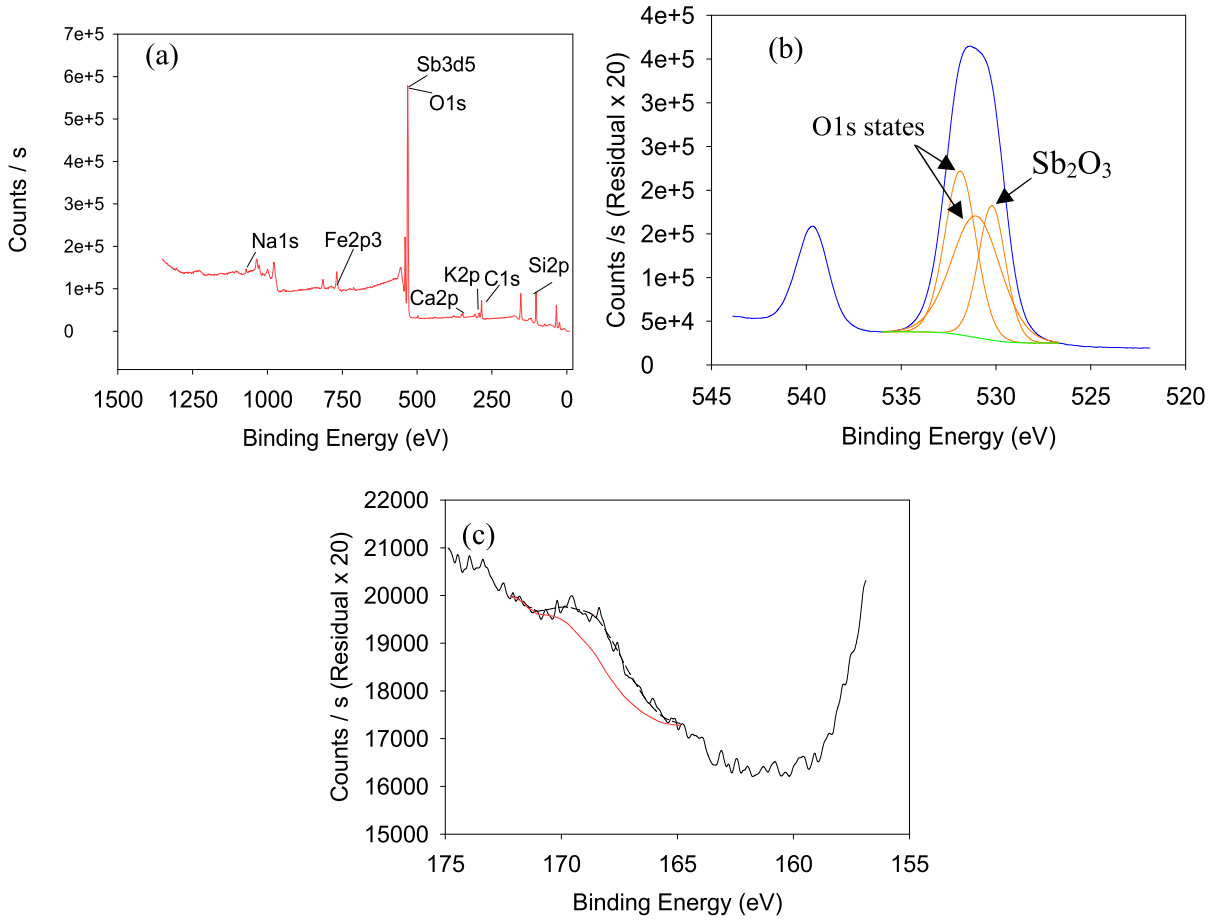

Fig. 2. XPS analyses of the slag: (a) general survey spectrum, (b) elemental spectrum for Sb, and (c) elemental spectrum for S.

(1) Raw material characterization and grinding, (2) Preliminary leaching test to determine the range of leaching parameters, (3) Extraction of Sb and REEs from the slag in the presence of HCl acid under atmospheric conditions, and (4) Recovery of Sb from the PLS via hydrolysis test.

2. Materials and methods

2.1. Materials

The slag was provided by Anadolu Antimon Factory, located in Adana, Türkiye. The slag is the by-products of Sb_2O_3 production process from a Sb-bearing ore via the pyrometallurgical process. Approximately 3 tons of slag were collected from various pre-identified locations within the stockpile with the aid of an excavator (Figure S1). These locations were chosen based on random sampling points. Subsequently, the collected material was subjected to cone and quartering techniques to obtain a final sample (400 kg).

The chemical composition of the slag (except for Si) was determined by an Atomic Absorption Spectrometer (AAS, Perkin Elmer 900H) after its digestion in a microwave digester (CEM, Mars 6) with a mixture of HF+HCl + HNO_3 + H_2O at 200 °C for 30 min, followed by boric acid neutralization at 200 °C for 30 min. Inductively Coupled Plasma – Optical Emission Spectrometry (ICP-OES, Perkin Elmer 7000DV) was employed to confirm the accuracy of the AAS results. X-ray Fluorescence (XRF, Panalytical MiniPal) analysis was performed on the slag for compositional analysis. XRF analysis (Thermo Scientific) at Anadolu Antimony Factory further confirmed the contents of antimony (Sb) and arsenic (As) in the slag. Table 1 details the chemical composition of the slag determined by AAS, ICP-OES and XRF, while its rare earth elements (REEs) and other elements concentrations given in Table 2 were measured by ICP-MS (Perkin Elmer, NEXION 2000P).

The slag sample was also analyzed for their gold (Au) and silver (Ag) content due to their potential [41,50,51]. The Au and Ag concentrations in the slag were determined as 3.70 g/t and 23.70 g/t, respectively. The chemicals (HCl, HNO_3, H_2SO_4, NaOH, NH_4OH, and tartaric acid) used in this work are of analytical grade and were used without any purification.

2.2. Methods

The experimental process, comprises different stages, including characterization and grinding, preliminary leaching test, HCl leaching, and hydrolysis. These stages are explained below.

2.2.1. Raw material characterization

Firstly, a series of analyses were conducted to determine some physicochemical properties of the slag used in this work. Physicochemical analyses including color, pH, moisture, dried matter, loss on ignition and inorganic phase analysis (XRD), Toxic Characteristic Leaching Procedure (TCLP) [52], and Synthetic Precipitation Leaching Conditions (SPLP) [52], were conducted. The procedures of TCLP and SPLP methods are given in Table S1. The mineralogical composition of the slag was determined using a PANalytical EMPYREAN X-Ray diffractometer (XRD) equipped with Cu Kα radiation (λ = 1,54049 Å) in the 2θ range of 10–85° with a 0.02 step size, and the obtained diffraction pattern was evaluated using a PDXL software program for mineral identification. The surface morphology of the slag was evaluated using a scanning electron microscope (SEM, FEI Quanta 650 Field Emission). In addition, the presence of Au and Ag in the slag was proved by SEM. The particle size distribution of the slag using a Malvern Mastersizer (Hydro 2000 MU) was determined. The surface property of the slag was further

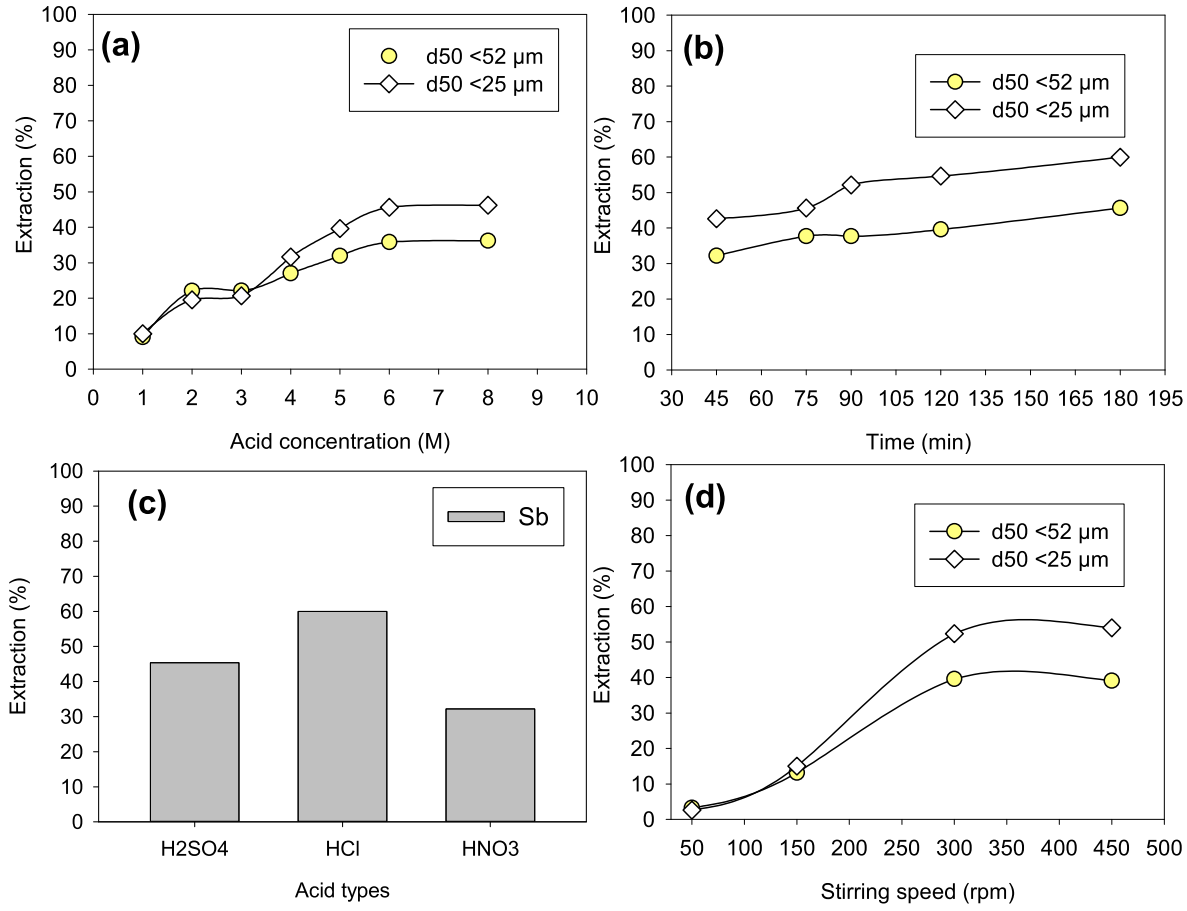

Fig. 3. The experimental findings obtained from preliminary leaching tests.

determined using X-Ray Photoelectron Spectroscopy (XPS, Thermo Scientific K-Alpha).

2.2.2. *Preliminary leaching tests*

In this stage, the slag was crushed using a lab-scale jaw crusher and ground in a ball mill for different times (1 h and 2 h). Therefore, the effects of particle size on the leaching behaviour of the slag were investigated. A series of preliminary leaching tests were carried out in a 500 mL glass jacketed reactor (equipped with a glass condenser) to determine the range of experimental parameters for the leaching of Sb from the slag. Different parameters, including particle size, acid type (H_2SO_4, HNO_3, and HCl), acid concentration, leaching time, and stirring speed, were investigated. Previous studies indicate that the leaching of Sb should be carried out at high temperatures to obtain satisfactory results. Considering these findings, reaction temperature and solid-to-liquid ratio were kept as 60 °C and 1:5, respectively. The reaction temperature was provided by a circulation water bath (JSR-22 T) and it was monitored by a laser thermometer. In each leaching test, a 200 mL of solution was used. The slurry was stirred by a magnetic stirrer (MTOPS MS300HS). At the end of the reaction time, the stirring was stopped, and the slurry was centrifuged (ELEKTRO-MAG M415 M) and filtered using Whatman 1 filter paper. The concentration of Sb in the pregnant leach solution (PLS) was analysed by AAS. The following equation was used to determine the extraction rate of Sb from the slag. The leaching residue was washed many times and dried at 105 °C in an oven (Memmert) for characterization tests.

$$E_{rate}(\%) = \frac{C_{PLS} \times V}{C_{SLAG} \times W} \times 100 \quad (1)$$

where E_{rate} is the extraction rate (%), C_{PLS} is the concentration of element in the PLS (mg/L), V is the final volume of the PLS (L), C_{SLAG} is the initial concentration of element in the slag (mg/kg), W is the amount of slag used in the leaching (kg)

2.2.3. *HCl leaching tests*

Considering preliminary leaching test results, HCl acid was selected as a leaching agent for this study. The effects of parameters on the leaching of Sb, REEs, and other elements identified as impurities from the slag were determined. The parameters with their levels are listed in Table 3.

It was decided to conduct leaching experiments based on the one-factor-at-a-time (OFAT) method. The concentration of Sb and other impurities (Al, K, Ca, Mg, Mn, and Si) from the slag was determined by AAS, while the amounts of REEs in the PLS after each leaching test were determined by ICP-MS (Perkin Elmer NEXION 2000P).

2.2.4. *Chemical kinetics*

A series of leaching experiments under the best conditions at different temperatures (20, 40, 60, and 75 °C) were carried out for different times. During the leaching, the sampling procedure was conducted in a certain time to observe the leaching behavior of the Sb. The obtained results for Sb leaching were evaluated using the shrinking core model, which is one of the most used approach to understand the leaching mechanism. Four different models with their equations are listed in Table 4.

The reaction rate constant was calculated, and the activation energy (E_a) was determined based on the best-shrinking core model.

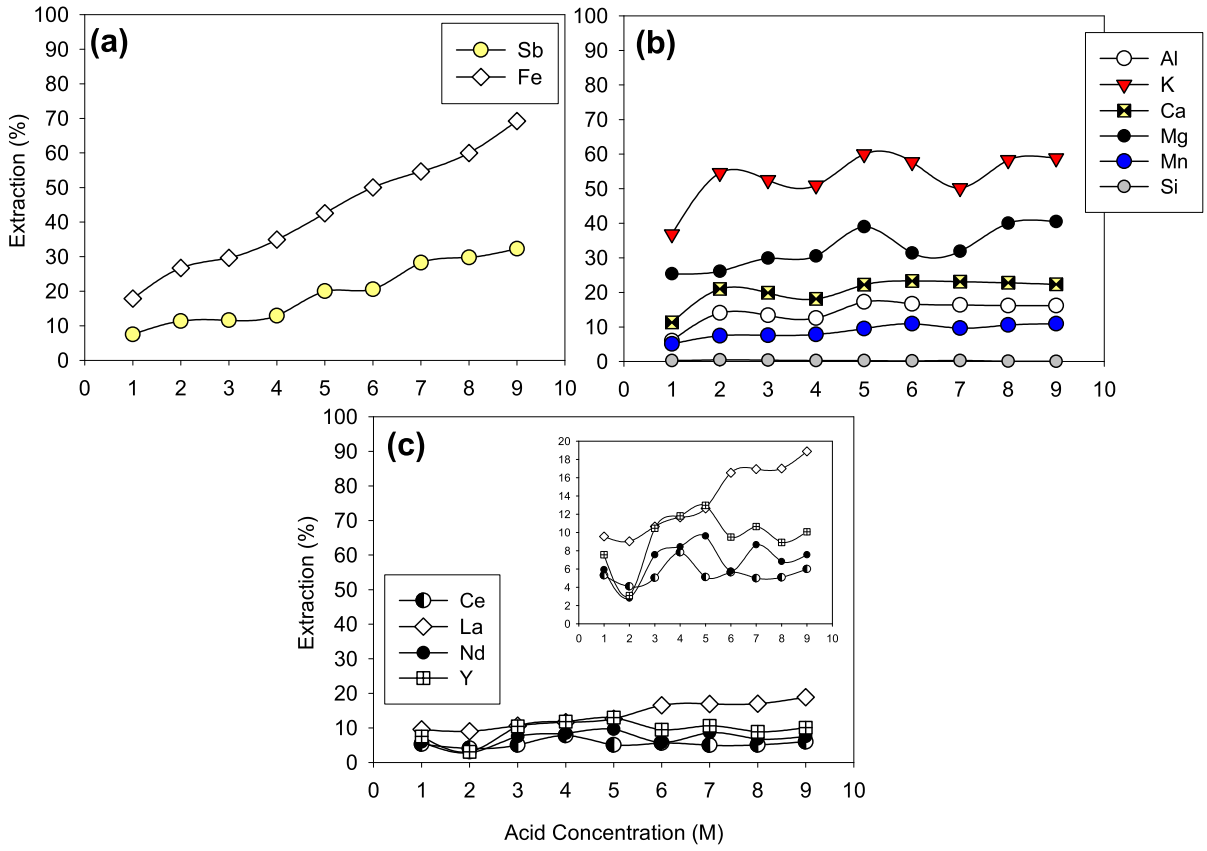

Fig. 4. The effects of acid concentration on the extraction rate of (a) Sb and Fe, (b) impurities, and (c) REEs from the slag.

Table 8
The effect of tartaric acid on the extraction rate of Sb.

Tartaric acid (g/L)	Extraction rate of Sb (%) HCl: 6 M	Extraction rate of Sb (%) HCl: 8 M
0	20.58	29.77
1	19.29	32.10
3	24.08	30.67
5	23.96	31.61
6	26.63	32.75

2.2.5. *Additional leaching tests for REEs*

Additional leaching tests were conducted for different times under optimum conditions to determine the effect of tartaric acid amount on the leaching behavior of La from the slag.

2.2.6. *Hydrolysis tests*

After the leaching tests, the PLS was prepared for the hydrolysis test. It was aimed to precipitate Sb with high precipitation rates with no Fe precipitation. Many parameters, including metal concentration, pH, and Cl concentration, played a crucial role in the hydrolysis process [44,53]. Furthermore, it was stated by previous researchers that the color of the obtained product may vary based on the alkaline types (NH_4OH, NaOH, and Na_2CO_3) [54]. As such, the Sb_2O_3 product obtained with the use of water was white, while yellowish Sb_2O_3 was obtained in the presence of NH_4OH. Herein, two different bases (NaOH and NH_4OH) were used. The hydrolysis tests were carried out based on the Taguchi approach (L32, 2^1 4^3). The experimental parameters with their levels are listed in Table 5.

Table 6 gives the experimental conditions for the hydrolysis test. In each hydrolysis test, the PLS with a volume of 100 mL was used. The pH of the PLS increased to the desired levels with the addition of two different alkaline (NH_4OH and NaOH). When the pH of the PLS reached the desired levels, the stirring was kept for an additional 30 min at the desired temperature. When the required time was over, solid-to-liquid separation was carried out using a centrifuge followed by Whatman 1 paper.

The concentrations of Sb and Fe in the solution after the hydrolysis were measured by AAS. The hydrolysis ratio of Sb was calculated using the following equation. The obtained precipitate was washed with hot water and dried at 105 °C for 1 h in an oven. An additional hot water leaching procedure (solid-to-liquid ratio: 1/10) was carried out at pH of 8 with the addition of alkaline (NH_4OH, 1 M) to remove the Cl content from the precipitate and therefore Sb-oxide could be obtained. The same drying procedure was conducted.

$$P_{rate} = 100 - \left(\frac{C \times V}{C_1 \times V_1} \times 100\right) \quad (2)$$

where P_{rate} is the hydrolysis ratio (%), C is the final concentration of the element after the hydrolysis (mg/L), V is the final volume of the solution after the hydrolysis (L), C_1 is the initial concentration of an element in the PLS before the hydrolysis (mg/L) and V_1 is the initial volume of the PLS (L).

The XRD patterns of the selected products were measured. Also, the polymorph properties of the selected products were examined by SEM. Additional hydrolysis tests were carried out for the optimization of the process according to the results obtained based on the Taguchi approach (Table 7).

3. Results and discussions

3.1. *Characterization of the slag*

The obtained results for the physicochemical properties of the slag

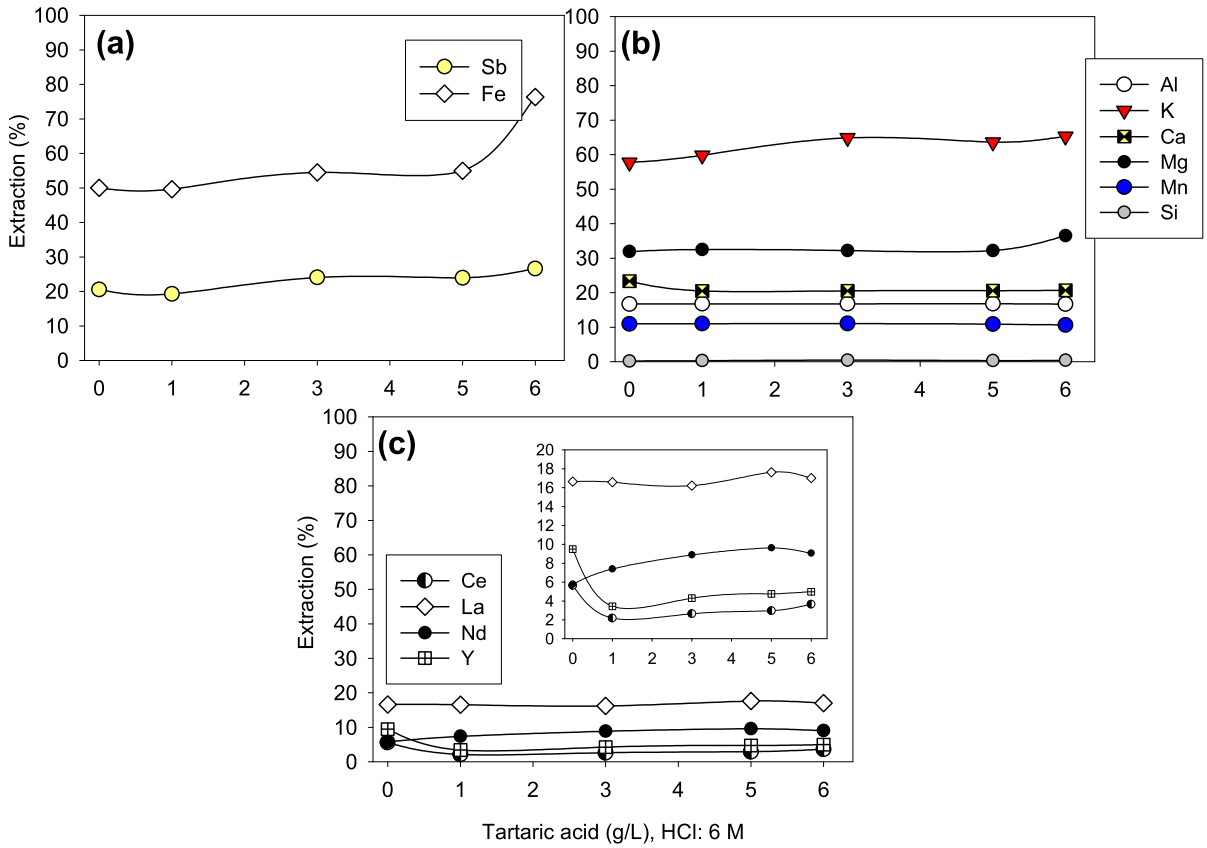

Fig. 5. The effects of tartaric acid on the extraction rate of (a) Sb and Fe, (b) impurities, and (c) REEs from the slag in the presence of 6 M HCl.

are summarized in Table S2. Many methods can be used to determine the toxicity properties of the slag generated in pyrometallurgical processes, and TCLP and SPLP methods are recommended [52,55]. The behaviour of organic acid (acetic acid) with a low molecular weight on the slag was determined in the TCLP method [56]. In contrast, acid rain's effect on the slag in the stock area was simulated in the SPLP procedure [57]. The difference between those methods was the chemicals used. Acetic acid was used in the TCLP, whereas a mixture of nitric-sulphuric acid was used in the SPLP. After conducting the TCLP method, the amount of dissolved Sb was 10.82 mg/L, corresponding to an extraction rate of 0.05 %. Although the amount of dissolved Sb was relatively lower than that of a previous study [14], it was thought that this value was higher than acceptable levels in drinking water. The amount of Sb dissolved in a mixture of HNO_3:H_2SO_4 acid was found to be 13.06 mg/L.

3.1.1. *Mineralogical composition of the slag*

It was determined that the dominant mineral in the slag sample is quartz (SiO_2) and it contains a relatively low amount of stibiconite ($Sb_3O_6(OH)$) mineral (Fig. 1). Detailed mineralogical analysis conducted using the Rietveld method revealed the presence of microline ($KAlSi_3O_8$), magnetite (Fe_3O_4, <%5), and hedenbergite ($CaFeSi_2O_6$) minerals within the slag. Due to the detection limit of XRD, peaks representing Sb metal could not be detected.

SEM analyses were carried out to evaluate the properties of the slag. Figure S2 shows the SEM images and EDX analyses taken from polished slag. It was determined that the slag has an inherently shapeless and amorphous structure. From an elemental content perspective, it was also observed that the Sb element under study forms compounds with different elements (S, O) and/or element groups (Fe, Al, Si, Na, Ca), has a very small particle size distribution, and cannot be obtained by conventional methods. The main element of the slag, consistent with XRD analysis, was determined to be quartz (SiO_2) through SEM images. Elements such as Ag and Th could be detected via BSE images, and their presence was confirmed by EDX analysis.

Fig. 2 shows the XPS spectra of the slag. Due to the overlapping of the O1s elemental spectrum with the $Sb_3d_{5/2}$ orbital during analysis, it was recommended to use the $Sb_3d_{3/2}$ spectrum for deconvolution analysis [58]. The presence of Na, Fe, Sb, Ca, K, and Si elements on the surface of the sample was detected in the general survey (Fig. 2 a). The binding energy of the characteristic peaks was found to be 102.8 eV for Si2p, 532.2 eV for Sb3d5, 284.4 eV for C1s, 293.54 eV for K2p, 1071.31 eV for Na1s, 347.52 eV for Ca2p, 711.12 eV for Fe2p3, and 531.2 eV for O1s. The presence of C1 observed in the analysis is attributed to carbon contamination. It was calculated from Fig. 2 a that the atomic weights of Sb3d5 and O1s was found to be 63.07 % and 21.9 %, respectively.

As a result of the analysis, the presence of an oxide peak attributed to the $Sb_3d_{3/2}$ orbital within the O1s peak was identified (Fig. 2 b). The elemental spectrum shown in blue represents the lower limit of the integral obtained after background correction, while the reddish peaks represent the deconvoluted peaks resulting from the analysis. Thus, the O1s and $Sb_3d_{5/2}$ orbitals yielded three peaks, one of which (approximately 9.4 eV apart from $Sb_3d_{3/2}$) is attributed to Sb oxide, while the other two belong to the O element. Three different Sb oxides are known: Sb_2O_3 (Sb^{3+}), Sb_2O_4 (Sb^{4+}), and Sb_2O_5 (Sb^{5+}). The representation of the $Sb_3d_{3/2}$ spectrum with only one peak indicates that the Sb element present in the slag sample used in the study is in the form of Sb_2O_3 [59,60]. Although no evidence of metallic Sb or other Sb oxide minerals was obtained in the slag by XRD and XPS, it was observed that some slag phases are wrapped around the antimony phase and that the wrapped antimony phase is mainly metallic antimony (see Figure S2). The low amount of sulfur (S) detected on the sample surface did not allow any inferences regarding an interaction between S and Sb (Fig. 2 c).

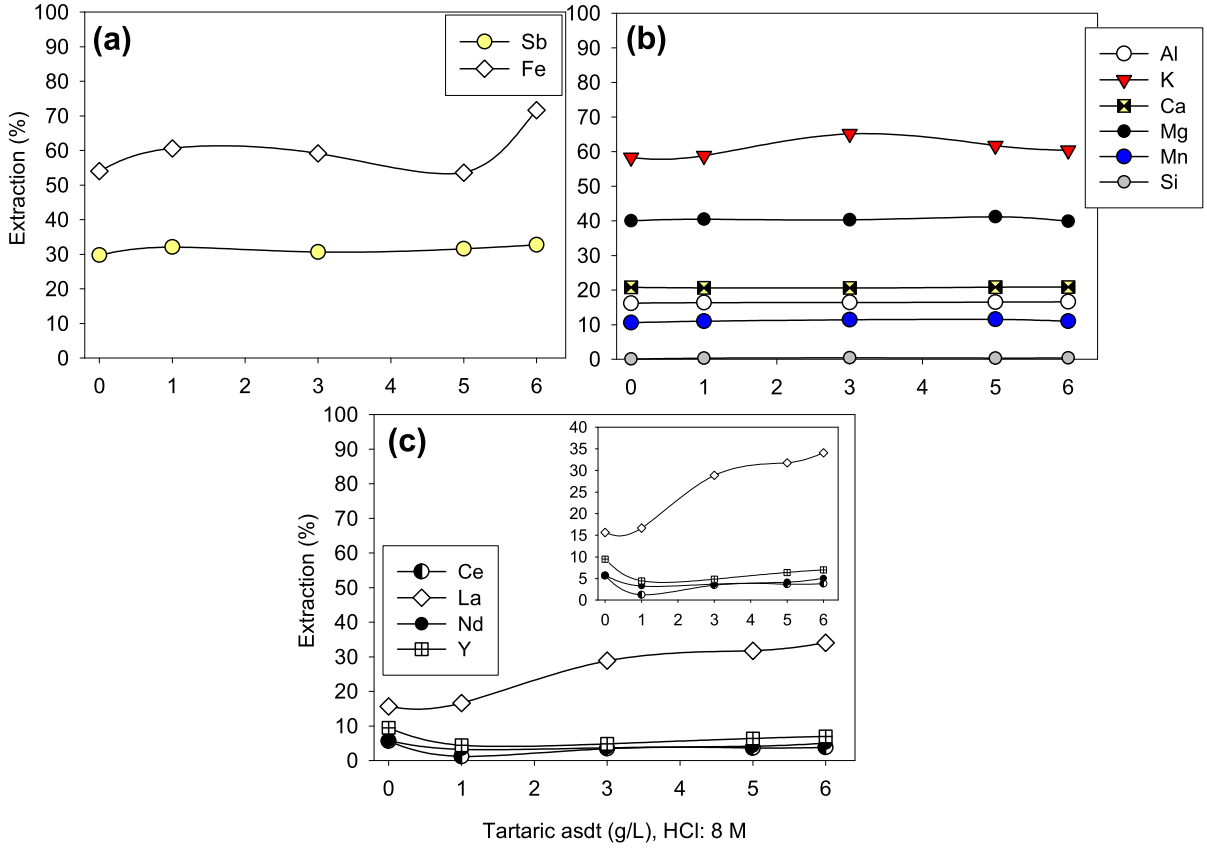

Fig. 6. The effects of tartaric acid on the extraction rate of (a) Sb and Fe, (b) impurities, and (c) REEs from the slag in the presence of 8 M HCl.

3.2. Results of preliminary leaching tests

The ore collected from a smelter plant and brought to the laboratory was crushed by a jaw crusher and ground in a ball mill for two different time intervals. The particle size distributions of the ground slag are shown in Figure S3. The average particle sizes (d_{50}) of the slag prepared for the leaching test were found to be 24.5 μm and 51.55 μm, respectively. It is clear from Figure S3 that the uniformity of the product is satisfying. Previous researchers show Eh-pH diagram of Sb-based species in acidic solutions at 25 °C [38]. Using this diagram, the phase conversion of Sb can be predicted during the leaching. It is seen that an acidic and positive-potential conditions are necessary for the leaching of Sb. Although HCl was suggested as the best leaching agent for Sb, herein HNO_3 and H_2SO_4 were used for comparison. The effects of particle size on the extraction of Sb from the slag were investigated under the following conditions: a reaction temperature of 60 °C, a time of 45 min, a solid-to-liquid ratio of 1/5, and a stirring speed of 300 rpm. Fig. 3 reveals the preliminary experimental findings for the leaching of Sb from the slag. It was determined that a decrease in the particle size led to an increase in the extraction rate of Sb as shown in Fig. 3(a). The extraction rate of Sb from the slag increased in parallel with the increase of HCl. For example, the extraction rate of Sb from the slag was around 10 % in the presence of 1 M HCl, but its extraction rate increased up to 50 % depending on HCl concentration. However, these values are highly dependent on the particle size. The Sb with an extraction rate of 45 % was dissolved from the slag with an average particle size of 25 μm in the presence of 6 M HCl, whereas the extraction rate of Sb was found to be around 35 % from the slag with an average particle size of 52 μm under the same conditions. As expected, the Sb extraction rate increased over an extended time (Fig. 3(b)). For example, an increase in the reaction time from 45 min to 180 min led to obtain high Sb extraction rates, which are 59 % and 45 % for the slags with an average particle size of 24.5 μ m and 51.55 μ m, respectively.

Fig. 3(c-d) show the effect of acid types and stirring speed on the extraction of Sb from the slag ground for two different times. In these tests, the following parameters were kept constant: acid concentration of 6 M, time of 180 min, solid-to-liquid ratio of 1/5, and temperature of 60 °C. The extraction rate of Sb in the presence of HCl was found to be > 50 %, which was higher than other inorganic acids (H_2SO_4 and HNO_3). In the leaching process, mixing the slurry at a controlled rate enhances the interaction between the leaching agent and the solid, thereby prolonging their contact time. This augmentation in the hydrodynamic behavior of the leaching system leads to a reduction in the thickness of the liquid boundary layer, consequently bolstering leaching efficiency.

As shown in Fig. 3(d), the positive influence of increased agitation speed on Sb dissolution was determined. The intensified interaction between particles and the leaching agent is evident, corresponding to higher stirring speeds. However, experiments conducted at speeds exceeding 300 rpm revealed a limited increase in Sb dissolution efficiency. It can be inferred that the augmentation in extraction efficiency, attributed to vortex formation dependent on stirring speed, is achieved by elevating it from 150 rpm to 300 rpm. Similar findings were seen in the literature. Aktaş and Çetiner [61] demonstrated that a speed of 200 rpm is adequate for vortex formation and subsequent Sb dissolution, with no discernible change in efficiency observed at higher speeds.

Previous researchers show the Eh-log[Cl^-] diagram of the Sb-Cl-H_2O system at ambient temperature [62]. It is seen in their study that an increase of the Cl^- ions in the leaching system triggered the increase in the extraction rate of Sb from the slag, compared to that of other leaching agents (see Fig. 3(b)). These findings are proved by previous study [63], which indicates that Sb (III) species may form chloro-complexes, and its solubility increases within increasing Cl^- ions

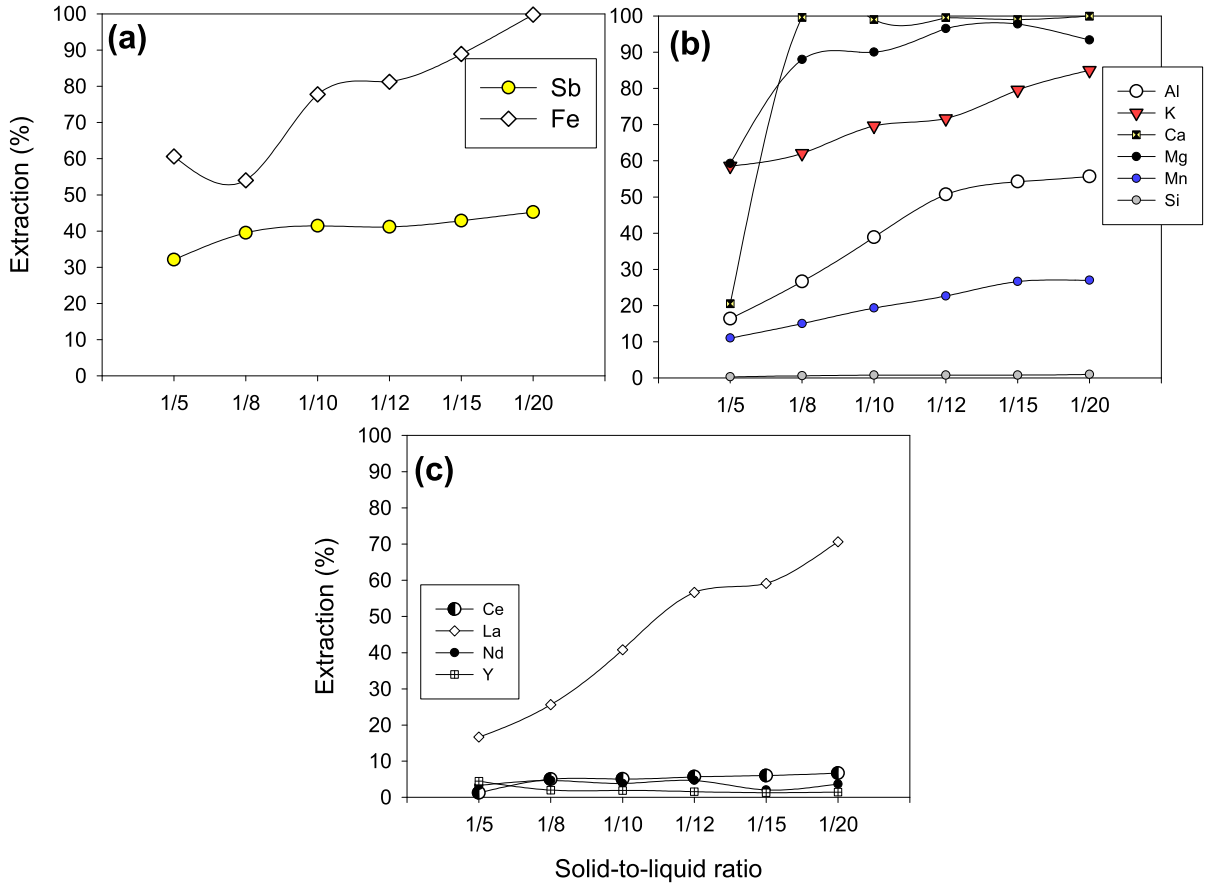

Fig. 7. The effects of solid-to-liquid ratio on the extraction rate of (a) Sb and Fe, (b) impurities, and (c) REEs from the slag.

activity. Therefore, it was decided to use HCl as the leaching agent not only to increase the extraction rate of Sb but also to decrease the re-precipitation of Sb during leaching. After preliminary leaching tests, the slag was prepared with a size of < 25 μ m in a ball mill for use in the subsequent leaching tests.

3.3. Results of HCl leaching tests

Hu et al. [46] suggested that leaching experiments should be carried out to extract Sb from raw materials at higher reaction temperatures. The following equation represents the possible leaching reaction.

$$Sb_3O_6(OH) + 12HCl \rightarrow 3SbCl_3 + 6H_2O + 3Cl \quad (3)$$

In these tests, the effects of the acid concentration, tartaric acid amount, solid-to-liquid ratio, reaction temperature, and time on the extraction of Sb from the slag were investigated. Furthermore, the leaching behaviours of the impurities and REEs were examined.

3.3.1. Effect of acid concentration

First, the effects of the acid concentration (1, 2, 3, 4, 5, 6, 7, 8, and 9 M) on the extraction of Sb from the slag (<25 μm) were determined in the presence of HCl. The strength of the acid concentration plays a crucial role in the leaching process. Other parameters, which were constant, were a reaction time of 45 min, reaction temperature of 60 °C, solid-to-liquid ratio of 1/5, and stirring speed of 300 rpm. An increase in the acid concentration caused the PLS to become yellowish from colorless (Figure S4). These changes in PLS color indicate the dissolution of Sb and other elements. The extraction rates of Sb and other elements (Al, K, Ca, Mg, Mn, and Si) from the slag are shown in Fig. 4. Sb and Fe extraction rates showed a linearly increasing trend with increasing acid concentration. However, the extraction rate of Fe was more than two times higher (69 %) than that of Sb (32 %) in the presence of the highest HCl concentration (9 M), as shown in Fig. 4.10(a). Previous studies have indicated that the HCl concentration should be high for the extraction of Sb; otherwise, dissolved Sb may be hydrolyzed depending on time, and therefore, the extraction rate of Sb from the slag started to decrease [64].

Based on the experimental findings, leaching tests were performed for the subsequent stages in the presence of 6 and 8 M HCl. Moreover, the extraction rates of other impurities were lower than 30 % (Fig. 4.4 (b)). Fig. 4.4(c) shows that the leaching behaviors of REEs were quite below (<10 %) even at the highest HCl concentration, except for La, for which the extraction rate was 18 %.

3.3.2. Effect of tartaric acid amount

As mentioned above, Sb ions may be hydrolyzed, decreasing the extraction rate of Sb [39,40]. Therefore, the experimental findings were significantly influenced. Previous studies have indicated that adding tartaric acid makes Sb ions more stable in PLS during leaching [65]. With the addition of tartaric acid, Sb ions form the Sb-tartrate complex, which has a more negative potential than hydrogen ions and prevents the hydrolysis of Sb from the PLS. For this purpose, the effects of tartaric acid (0, 1, 2, 3, 5, and 6 g/L) on the extraction of Sb from the slag were determined in the presence of 6 and 8 M HCl. The experimental parameters that were kept constant were as follows: reaction time, 45 min; reaction temperature, 60 °C; solid-to-liquid ratio 1/5, and stirring speed, 300 rpm. The use of tartaric acid has a positive effect on the Sb extraction rate, as listed in Table 8.

Fig. 5 and Fig. 6 show the effect of tartaric acid on the extraction rates of Sb together with other elements and REEs from the slag. When the experimental findings were evaluated, it was observed that there

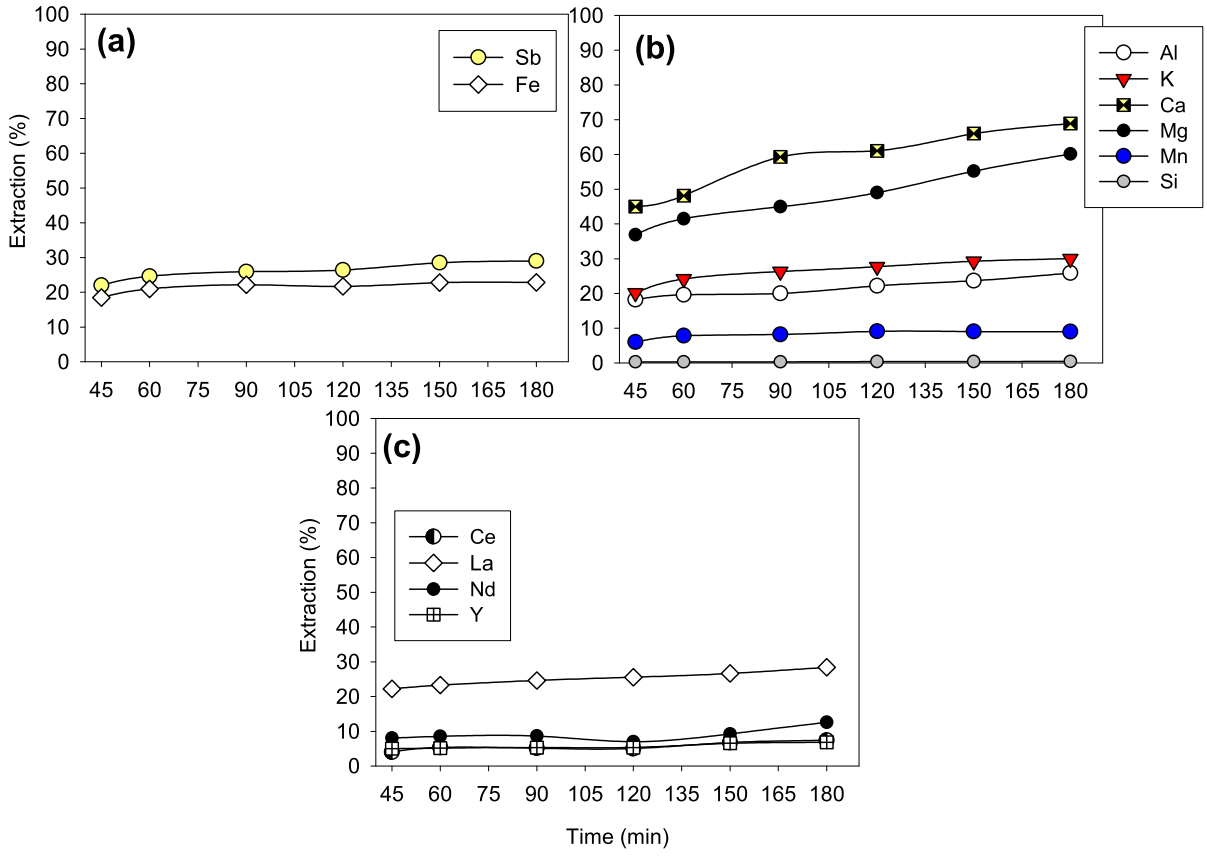

Fig. 8. The effects of reaction time on the extraction rate of (a) Sb and Fe, (b) impurities, and (c) REEs from the slag at ambient temperature.

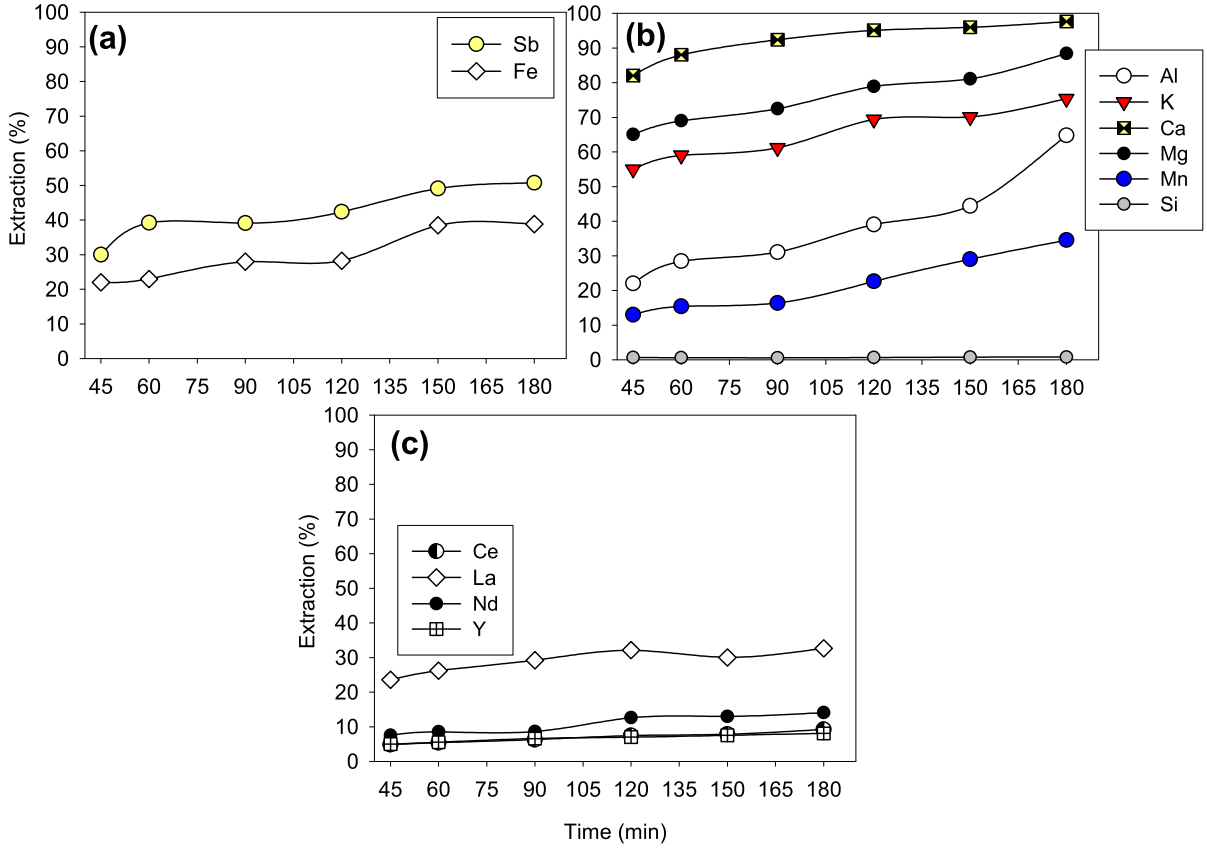

Fig. 9. The effects of reaction time on the extraction rate of (a) Sb and Fe, (b) impurities, and (c) REEs from the slag at a temperature of 40 °C.

was no effect on the extraction rate, except for La extraction. The increase in the extraction rate of La from the slag was due to the increase in the tartaric acid content. However, the increase in the extraction rates of other REEs (Ce, Y, and Nd) is negligible. In addition, the HCl concentration should be 8 M to extract La at high extraction rates in the presence of tartaric acid (6 g/L). Although there was no effect on the extraction rate of Sb in the presence of tartaric acid, tartaric acid was used at a concentration of 1 g/L in the subsequent leaching tests to minimize the possible hydrolysis of Sb ions. Additional leaching tests were performed to determine the effects of tartaric acid on the extraction rate of REEs in the subsequent stages.

3.3.3. *Effect of solid-to-liquid ratio*

Fig. 7 shows the effect of the solid-to-liquid ratio on the leaching efficiency. The experimental parameters were maintained at constant levels, including a reaction temperature of 60 °C, time of 45 min, HCl concentration of 8 M, and stirring speed of 300 rpm. The solid-to-liquid ratio plays a crucial role, with a decrease in the sample quantity per solvent concentration accelerating the dissolution process. As the solid-to-liquid ratio decreased from 1/5 to 1/20 under consistent experimental conditions, the extraction rate of Sb increased from 32 % to approximately 45 %. Notably, the extraction rate of Fe from the slag surpassed that of Sb, with nearly all Fe content passing into the solution under 1/20 solid-to-liquid ratio conditions (extraction rate > 99 %). Similarly, the extraction rate of impurities increased with decreasing solid-to-liquid ratio. For instance, the Ca and Mg extraction rate were higher than 90 %, whereas the Mn and Si was less than 25 % at a solid-to-liquid ratio of 1/20. On the other hand, Al and K extraction rate demonstrated an increasing trend with a decreasing solid-to-liquid ratio. As anticipated, a decrease in the solid-to-liquid ratio accelerated the extraction rate of La. However, no discernible differences in the extraction rates were observed for Ce, Nd, and Y.

3.3.4. *Effect of reaction time and temperature*

To investigate the effects of reaction time and temperature, a series of experiments were carried out at room temperature, 40 °C, 60 °C, and 75 °C for varying durations (45, 60, 90, 120, 150, and 180 min). Figs. 8–11 show the extraction rates of Sb and Fe as a function of time. Other parameters kept constant at this stage included an HCl concentration of 8 M, solid-to-liquid ratio of 1/10, tartaric acid amount of 1 g/L, and stirring speed of 300 rpm.

Experiments conducted at room temperature yielded very low extraction rates of Sb and Fe from the slag (<30 %). Despite increasing the reaction time from 45 to 180 min, no positive effect on the extraction rate was observed at room temperature (Fig. 5). These findings are consistent with those of Guo et al. [66], who reported limited extraction rates even with increased acid concentration and stirring speed at room temperature (Sb extraction rate < 30 %). It has been reported that a higher reaction temperature is required for highly efficient Sb extraction. For instance, experiments conducted at 40 °C with a reaction time of 45 min yielded an Sb extraction rate of approximately 40 %. In contrast, an increase in the reaction time, the extraction rate of Sb dissolution efficiency tended to increase from 40 % to approximately 80 %. Similarly, in these experiments, an increase in the dissolution efficiency of other impurities over time was observed. However, limited dissolution values were observed for REEs in the same experiment.

When the temperature was increased from 40 °C to 60 °C, almost all of the Fe contained in the slag had passed into the solution by the end of 180 min. An increase in the temperature led to an Sb extraction rate of approximately 80 % after 180 min. Palden et al. [16] also indicated that a temperature of at least 50 °C is necessary for the extraction rate of Sb from the slag. Therefore, the Sb dissolution behaviours observed in this study are consistent with those reported in the literature. Some studies have examined both Sb and Fe leaching behaviours. The results obtained in these studies differ from those of the present study in terms of the

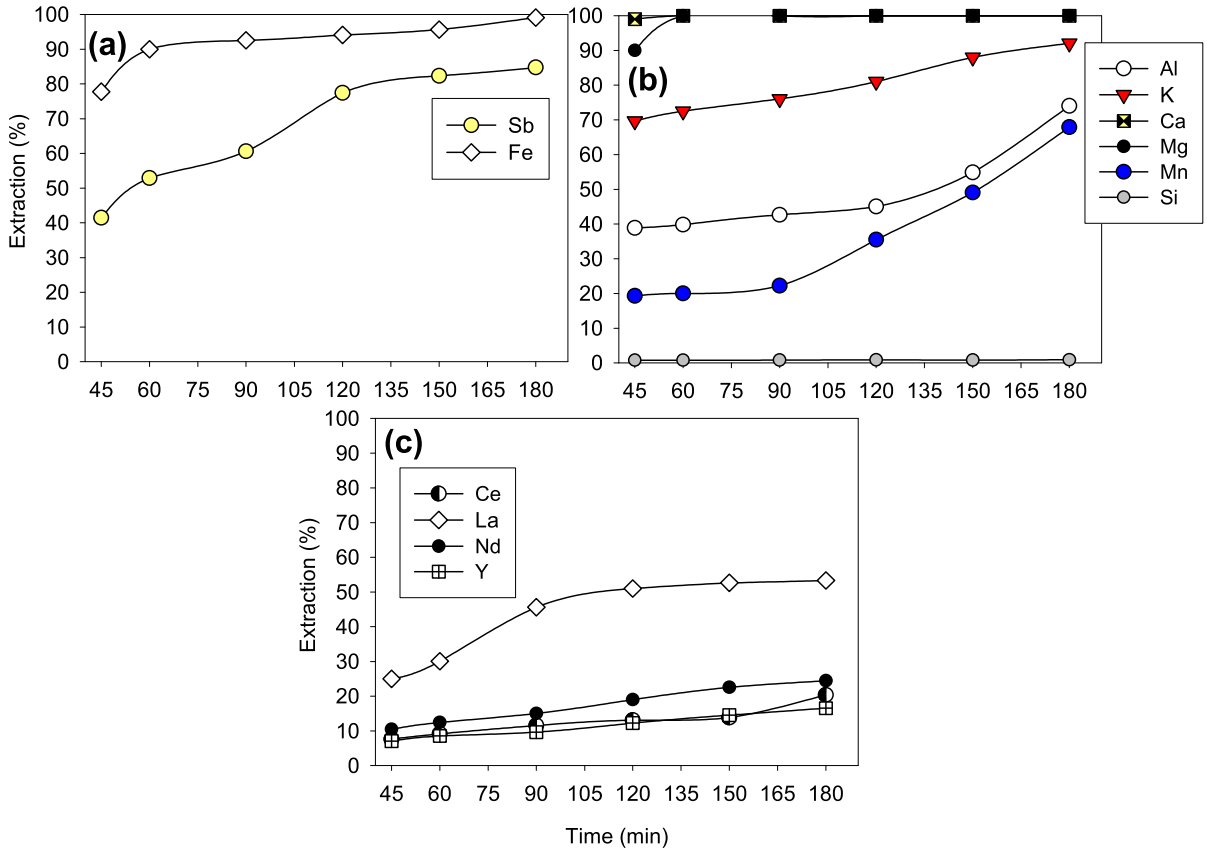

Fig. 10. The effects of reaction time on the extraction rate of (a) Sb and Fe, (b) impurities, and (c) REEs from the slag at a temperature of 60 °C.

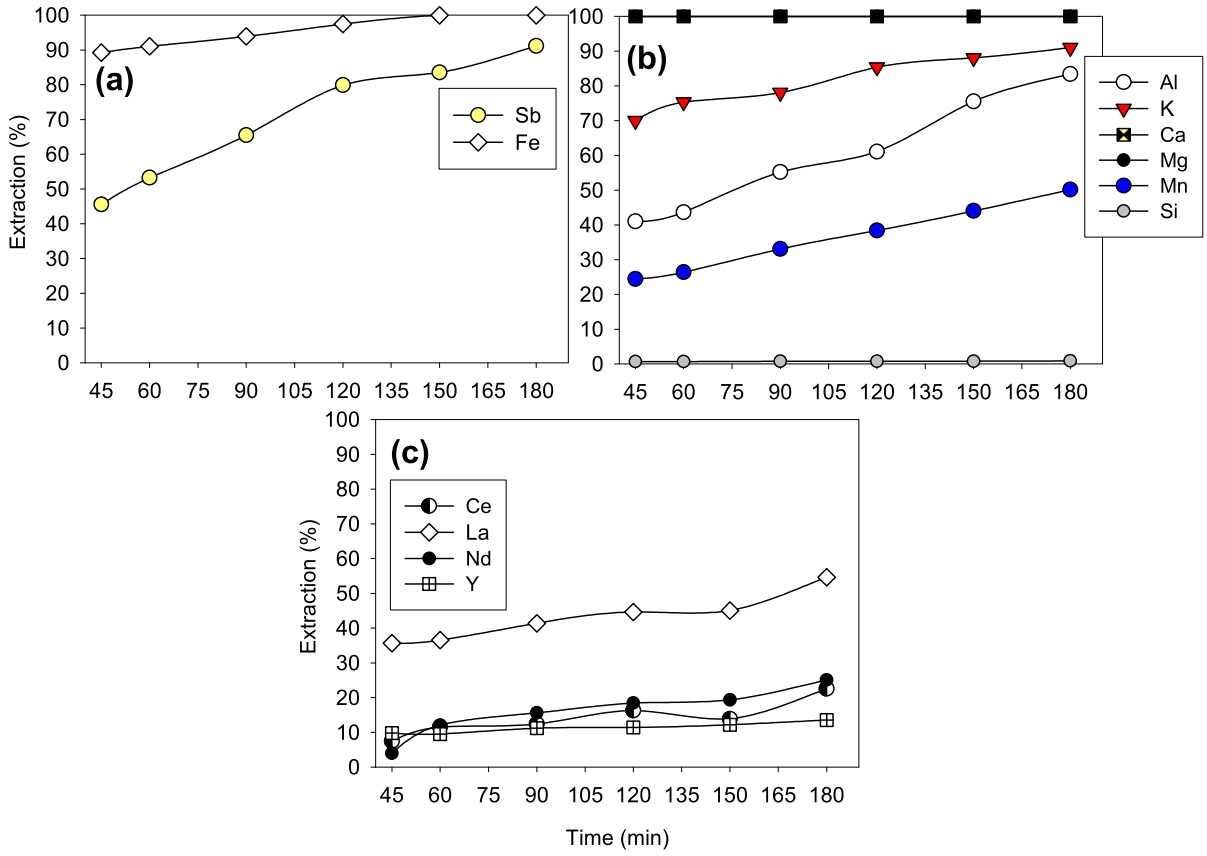

Fig. 11. The effects of reaction time on the extraction rate of (a) Sb and Fe, (b) impurities, and (c) REEs from the slag at a temperature of 75 °C.

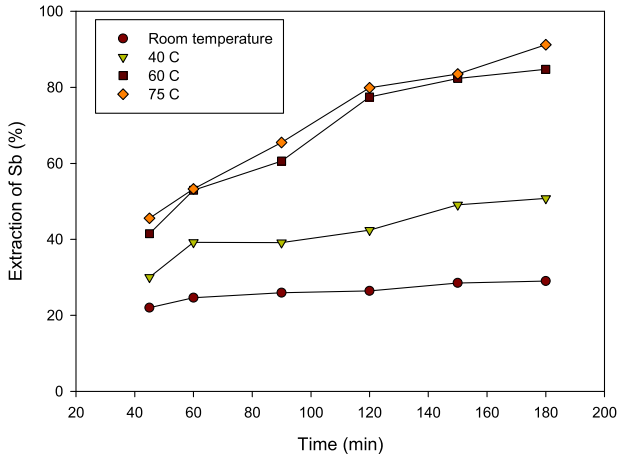

Fig. 12. The extraction rate of Sb from the slag at different temperatures.

extraction rate of Fe. Although high Sb dissolution values were achieved at high temperatures in the presence of HCl, they ensured very low levels of Fe passage into the solution. For example, during the dissolution of stibnite ore with HCl, the Sb dissolution efficiency was > 80 %, depending on the leaching conditions, whereas the Fe dissolution efficiency was less than 10 % [38]. This difference is thought to be due to the form of Fe in the raw materials.

As expected, as the temperature increased, Sb began to pass into the solution at the targeted levels, while the rates of undesirable impurities passing into the solution also increased, and almost all of the K, Ca, and Mg contained in the slag were dissolved. When the reaction temperature was 60 °C, the La dissolution efficiency of the slag was approximately 50 % after 180 min. However, no positive increase in Ce, Nd, and Y extraction rates was observed over time.

3.4. Results of kinetic study

Based on the experimental results, the leaching parameters required for achieving high efficiency in extracting Sb from the slag under atmospheric conditions are determined as follows: HCl concentration of 8 M, solid-to-liquid ratio of 1/10, stirring speed of 300 rpm, tartaric acid of 1 g/L, reaction temperature of 75 °C, and reaction time of 180 min. At this stage, the leaching experiments were conducted at different temperatures (room temperature, 40 °C, 60 °C, and 75 °C) and durations to elucidate the extraction behaviour of Sb during the leaching process. Experimental results obtained depending on time are shown in Fig. 12.

Leaching processes generally occur at the solid-to-liquid interface [67]. The occurrence of the stages in the leaching process depends on the physical and chemical properties of the solid particle targeted for dissolution, the type of solvent used, and the experimental conditions [68]. Therefore, mathematical modeling is an effective method used to determine the types of reactions and investigate leaching behaviours. The shrinking core model is one of the most commonly used mathematical models. With this method, values such as reaction type and reaction rate constant can be determined, and activation energy values for the dissolution reaction can also be calculated according to the most suitable chemical kinetic model. Thus, the most suitable kinetic model for the dissolution mechanism of Sb can be identified. Experimental results were evaluated using four different models (provided in Table 4); namely, (1) ash layer diffusion-controlled, (2) film diffusion-controlled, (3) surface reaction-controlled, and (4) both chemical and diffusion-controlled. The extraction rate of Sb from the slag depending on time, is converted into values that can be used in different kinetic models to

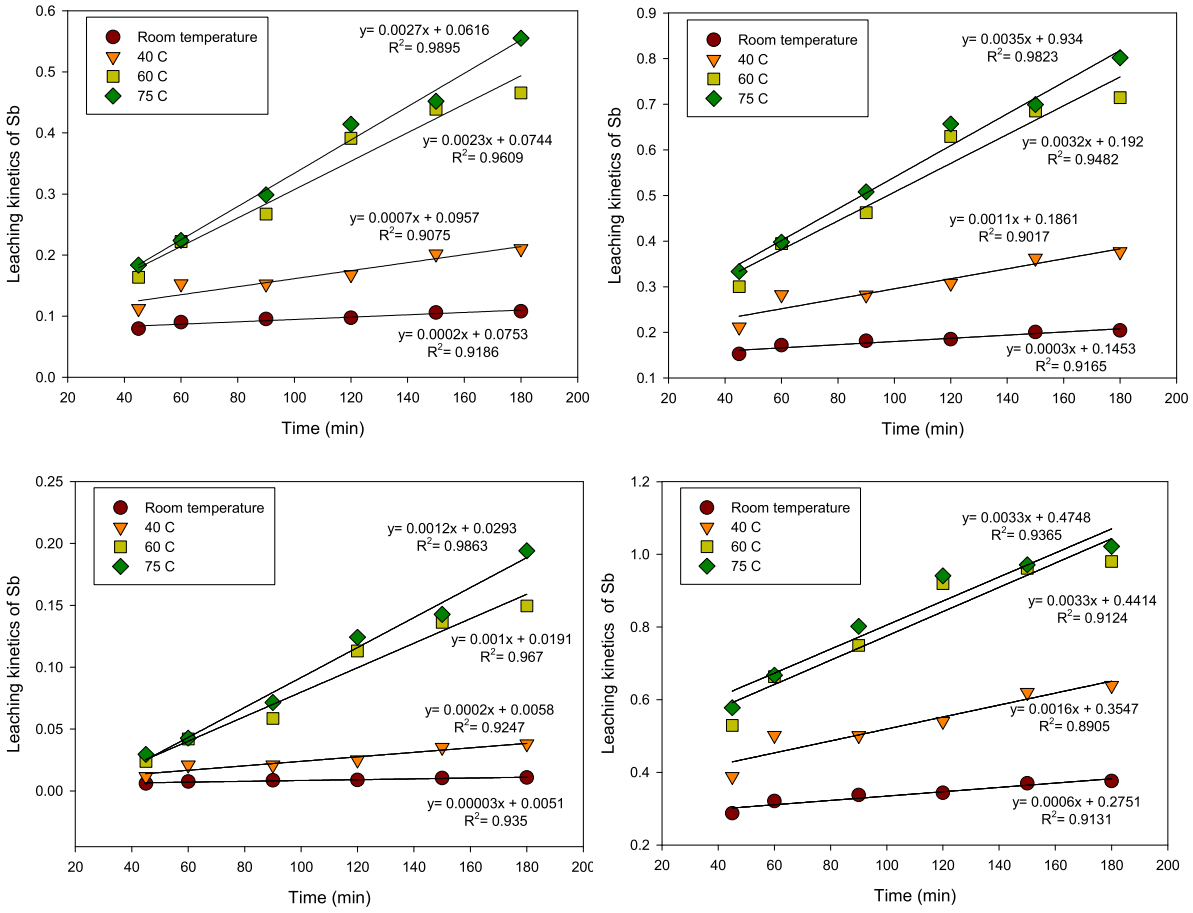

Fig. 13. Sb dissolution kinetics depending on time at different temperatures (a) Chemical reaction controlled model, (b) Film diffusion model (Jander equation), (c) Inner diffusion-controlled model, and (d) Both chemical and diffusion controlled model.

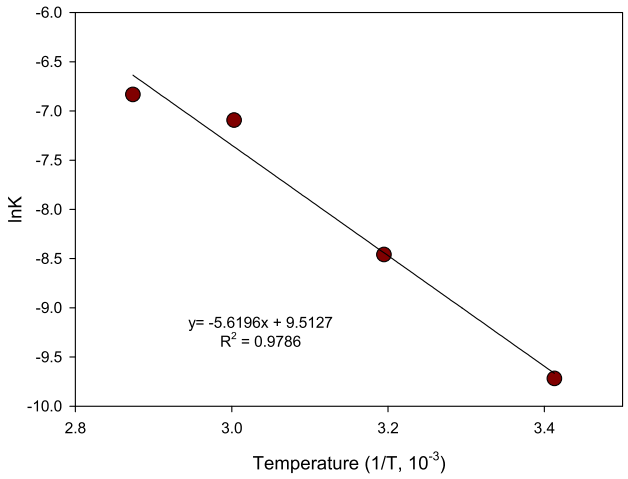

Fig. 14. Arrhenius curve for the extraction of Sb from the slag.

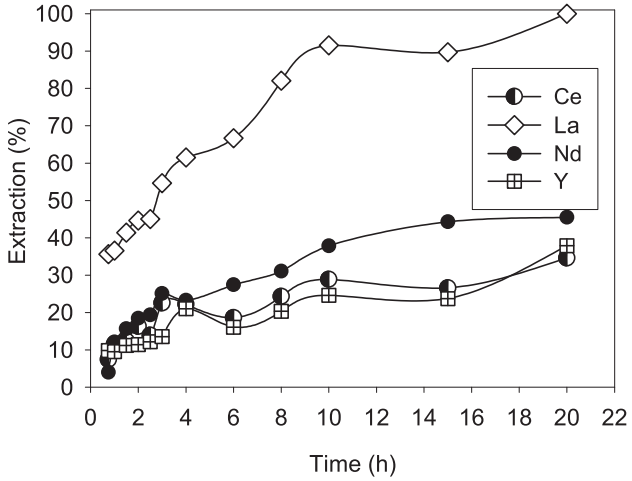

Fig. 15. The leaching behaviours of REEs under optimum conditions in extended leaching times (tartaric acid amount: 1 g/L).

explain the leaching behavior of the Sb. It was possible to evaluate the extraction mechanism of Sb as a function of temperature, as depicted in Fig. 13. In determining which of the four chemical kinetic models best explains the mechanism of Sb dissolution from the slag, particular attention has been paid to the R-squared (R^2) value. As observed, the R^2 value for each model is more significant than 0.90. The proximity of the R^2 values to 1 indicates that the experiments can be explained by these models. Considering the R^2 values obtained at each temperature, it has been concluded that the ash layer diffusion method is the best model for modeling the extraction of Sb from the slag.

The reaction rate constant values calculated from the slope values of these models. The reaction rate constant values in a range of between 6.01×10^{-5} min^{-1} and 107.84×10^{-5} min^{-1}, depending on the temperature. The Arrhenius curve was plotted using these reaction rate constants as shown in Fig. 14.

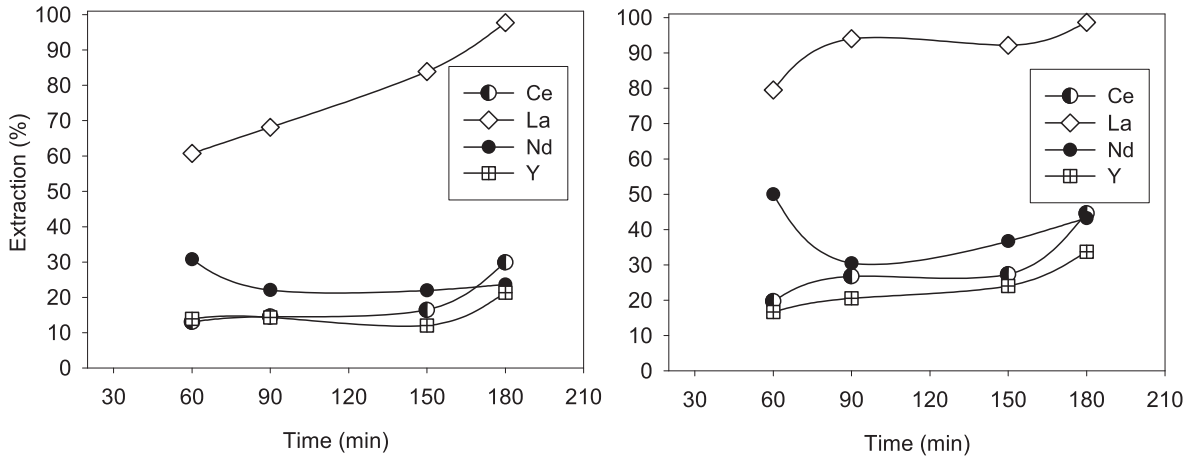

Fig. 16. Leaching behaviours of REEs from the slag under optimum conditions in extended leaching times (tartaric acid amount: 6 g/L).

Table 9
Experimental results obtained in the hydrolysis test.

Exp. No	Precipitation rate of Sb (%)	Precipitation rate of Fe (%)	Exp. No	Precipitation rate of Sb (%)	Precipitation rate of Fe (%)
1	90.38	25.12	17	99.38	98.83
2	80.62	63.69	18	92.48	85.91
3	93.09	87.05	19	79.76	62.08
4	94.00	91.00	20	81.36	29.65
5	53.86	13.54	21	88.03	79.52
6	66.02	36.32	22	82.02	66.31
7	73.87	51.03	23	79.03	55.11
8	85.00	91.00	24	65.51	38.21
9	50.91	8.02	25	71.51	55.35
10	47.78	2.14	26	84.82	80.36
11	89.09	79.55	27	60.76	35.21
12	71.64	46.87	28	72.60	57.14
13	55.75	17.09	29	89.31	82.46
14	55.92	17.41	30	90.86	88.27
15	89.91	81.10	31	59.55	26.70
16	75.45	53.99	32	68.35	42.72

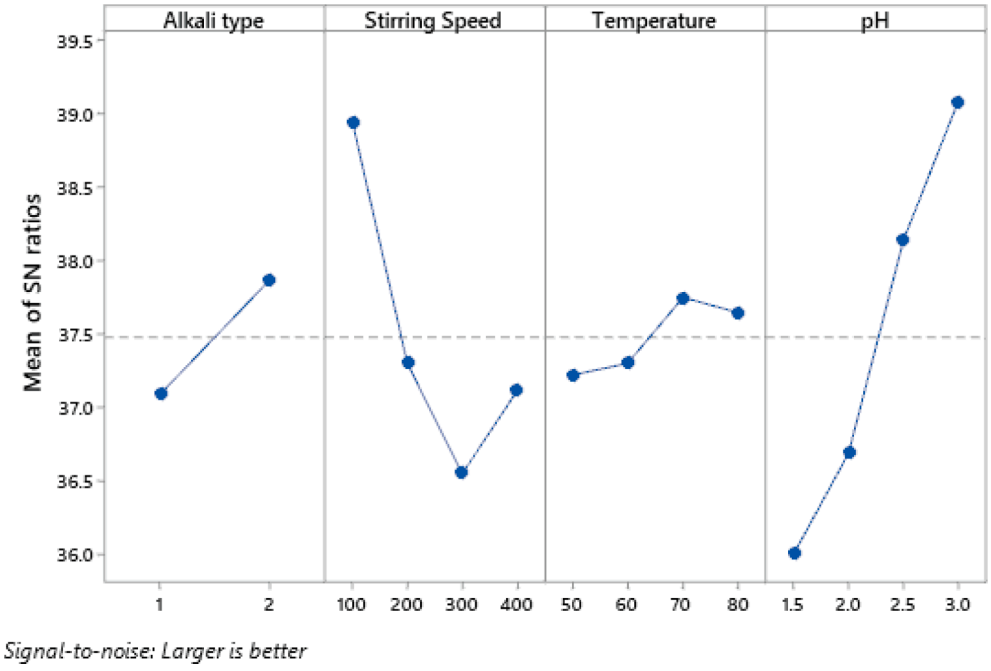

Fig. 17. S/N values of the experimental parameters for the precipitation of Sb from the PLS.

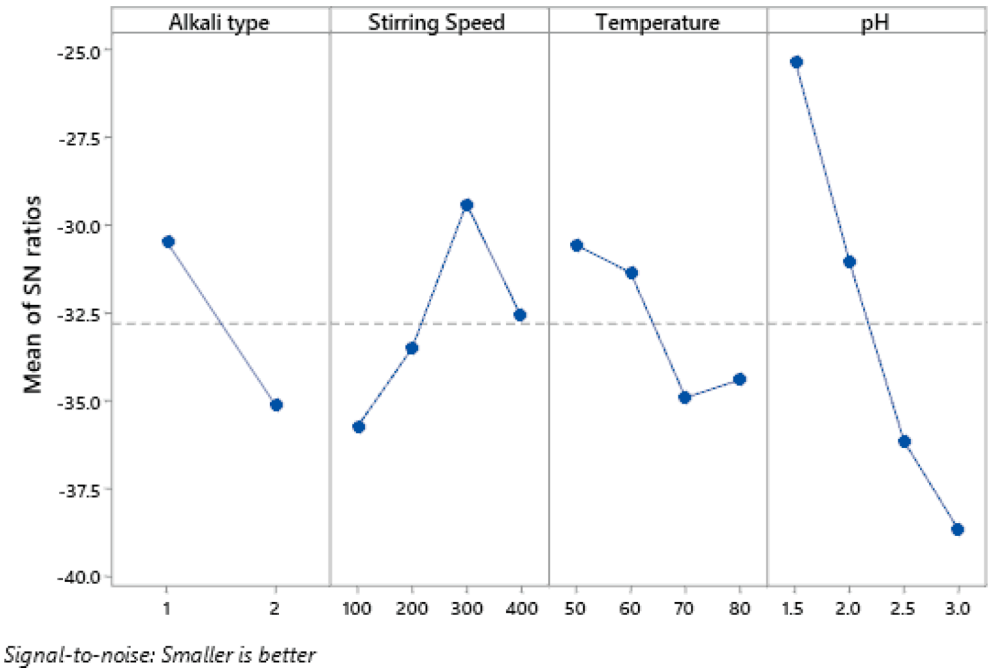

Fig. 18. S/N values of the experimental parameters for the precipitation of Fe from the PLS.

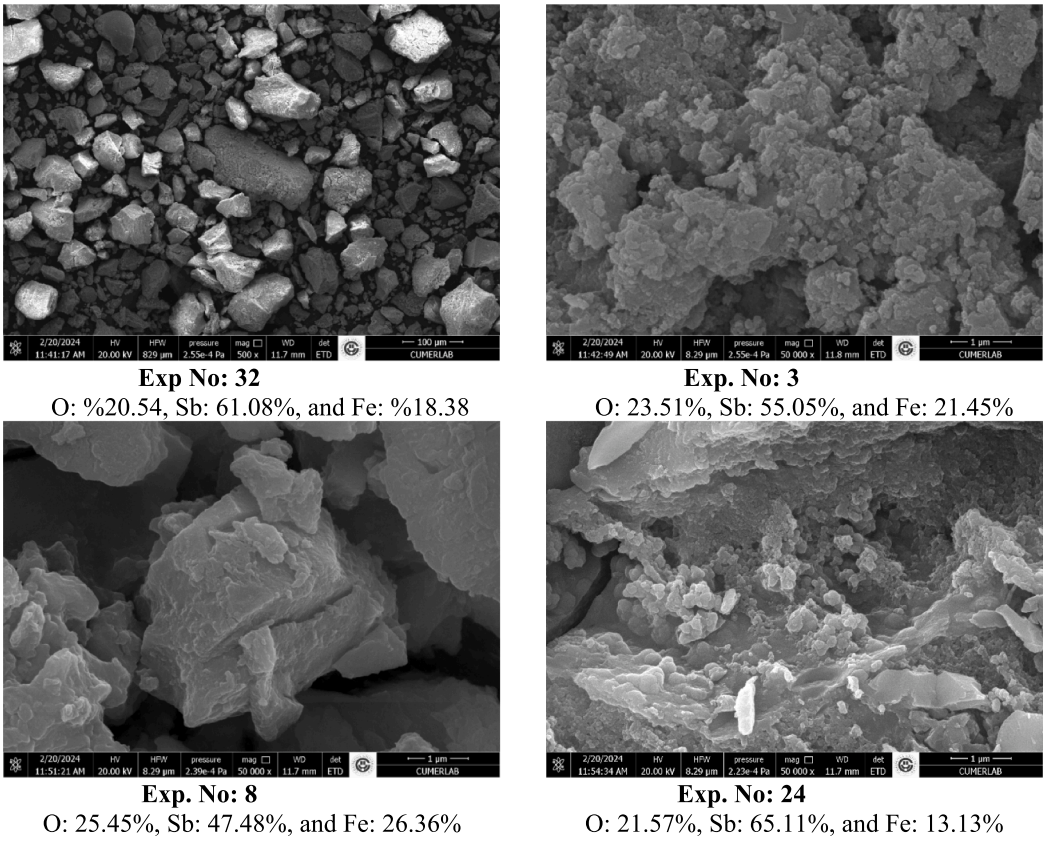

Fig. 19. SEM images of the selected precipitates and their chemical compositions determined by EDX.

The activation energy (E_a) can be calculated using the following equation. The conducted leaching reactions are classified based on their Ea values. For example, if $E_a < 20$ kJ/mol, the reaction was governed by a diffusion-controlled mechanism. Conversely, if $E_a > 42$ kJ/mol, it indicates an exponential relationship between the rate constant and temperature, the leaching mechanism can be explained by a chemically controlled mechanism [68]. The E_a was calculated to be 46.75 kJ/mol, which indicates that the chemically controlled mechanism governed the leaching of Sb from the slag.

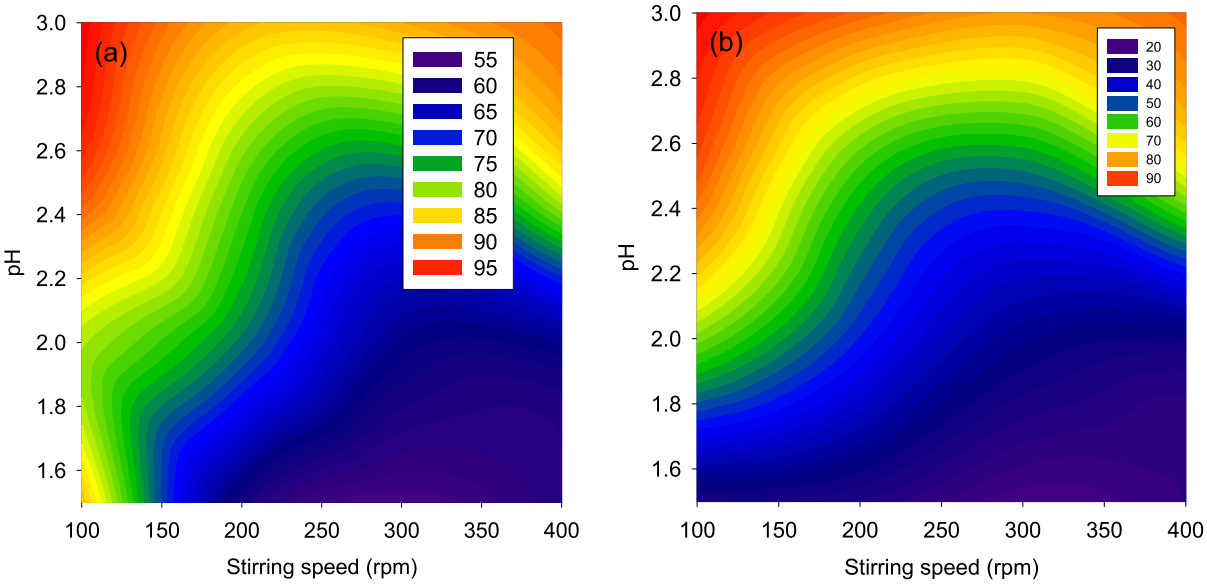

Fig. 20. Contour diagrams that show the effects on pH and stirring speed on the hydrolysis of Sb and Fe from the PLS (a) the precipitation rate of Sb and (b) the precipitation rate of Fe.

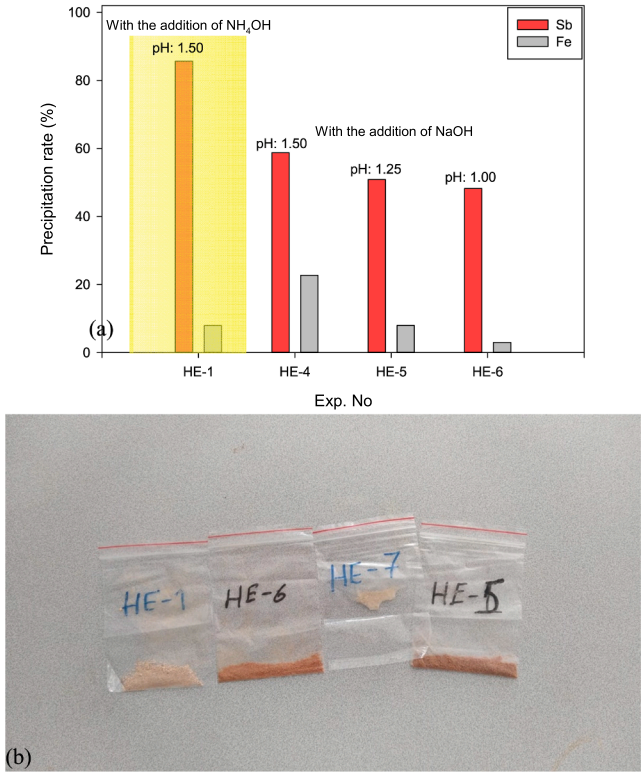

Fig. 21. (a) The precipitation rate of Sb and Fe from the PLS in the additional hydrolysis test (b) Photographs of the obtained precipitates.

$$k = A_o e^{\frac{-E_a}{RT}} \quad (4)$$

3.5. Results of additional leaching tests for REEs

It was determined that the addition of tartaric acid not only prevented the hydrolysis of dissolved Sb ions but also positively contributed to the extraction of La from the slag. In previous stages, the extraction rate of La from the slag was around 50 % under optimum leaching conditions (see Fig. 11). Therefore, it was decided to conduct leaching experiments in extended times. The parameters that are kept constant in these experiments were as follows: HCl concentration: 8 M, solid-to-liquid ratio: 1/10, stirring speed: 300 rpm, tartaric acid concentration: 1 g/L, and reaction temperature: 60 °C. The experimental results can be seen in Fig. 15. It was determined that a leaching time of 20 h is required for the complete extraction of La contained in the slag. The extraction rates of other REEs (Ce, Y, and Nd) under the same conditions are in the range of 25 – 40 %.

Additional leaching experiments at a temperature of 60 and 75 °C were conducted to determine the effect of tartaric acid amount on the extraction of REEs from the slag, respectively. An increase in the amount of tartaric acid makes the extraction of La with high rates in shorter times. While the experiments conducted with 1 g/L tartaric acid determined a leaching time of 20 h for the complete extraction of La, increasing the tartaric acid concentration from 1 g/L to 6 g/L reduced the time required for high-efficiency dissolution of La to 180 min (Fig. 16). These findings are consistent with previous studies [69], which reveal that the required time for the extraction of La from the soil decreased with the increase of tartaric acid concentration in the leaching system.

Under these applied conditions, the extraction rate of Sb from the slag was determined to be 91.19 %. While the extraction rate of La was approximately 97 %, the extraction rates of other REEs (Y, Ce, Nd) were measured to be $\leq$ 50 %.

3.6. Results of hydrolysis tests

This technique is used for the recovery of Sb from the PLS. In this process, Sb ions are hydrolyzed with different precipitators (water or alkaline) at a specific temperature. The possible chemical reactions during the hydrolysis process are explained in Equations 5–8.

$$4SbCl_3 + 5H_2O \rightarrow Sb_4O_5Cl_2\downarrow + 10HCl \quad (5)$$

$$Sb_4O_5Cl_2 + 2NH_4OH \rightarrow 2Sb_2O_3 + 2NH_4Cl + H_2O \quad (6)$$

$$Sb_4O_5Cl_2 + 2NaOH \rightarrow 2Sb_2O_3 + 2NaCl + H_2O \quad (7)$$

$$Sb_4O_5Cl_2 + Na_2CO_3 \rightarrow 2Sb_2O_3 + 2NaCl + CO_2 \quad (8)$$

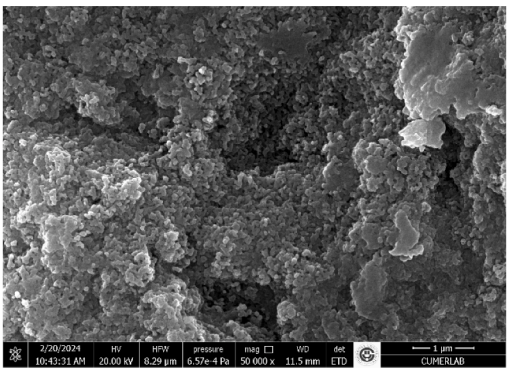

Exp. No: HE-5

O: 10.95%, Sb: 36.09%, Cl: 42.97%, and Fe: 9.93%

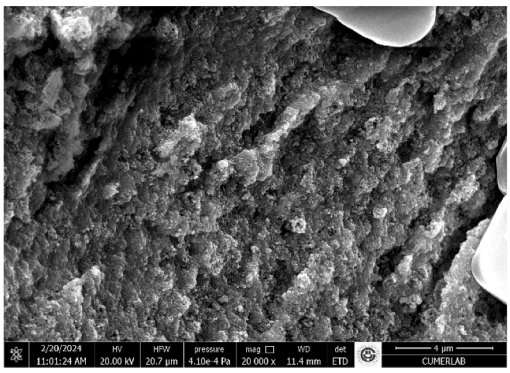

Exp. No: HE-6

O: 15.28%, Sb: 16.81%, Cl: 65.02%, and Fe: 2.89%

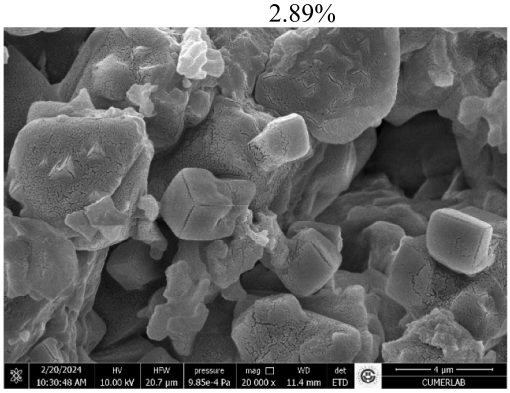

Exp. No: HE-1

O: 10.23%, Sb: 47.13%, Cl: 40.13%, and Fe: 2.51%

Fig. 22. SEM images of the selected precipitates obtained in the additional hydrolysis test and their chemical compositions determined by EDX prior to conducting the washing procedure.

As seen in Equation (5), HCl formed in line with the production of $Sb_4O_5Cl_2$ particles, and therefore the pH of the solution increased slowly [38]. Uysal [70] indicates that the concentration of Cl^- and OH^- ions determines the stability of $SbCl_3$ system. A mixture of Sb-products was obtained based on Sb^{3+} and Cl^- concentrations [45]. Depending on the equilibrium changes, Sb ions may form a precipitate or the precipitate obtained may dissolve again. Different Sb compounds ($Sb_4O_5Cl_2$, Sb_2O_3, and SbOCl) were formed based on the process [71,72]. It was known that $SbCl_3$ undergoes hydrolysis in water to form SbOCl. With the addition of bases, $Sb_4O_5Cl_2$ is formed in the presence of tartaric and HCl acids. The theoretical prediction for the hydrolysis product depending on the pH was shown in those of a previous study [73]. It is known that other impurities (Al, K, Mg, Na, Mn) present in the PLS did not decrease the purity of the precipitate obtained after the hydrolysis because all impurities are in ion form in the PLS, except for Fe ions that start to precipitate in these pH range (0 – 4). The precipitation behaviours of these metals depending on the pH value can be seen in Figure S5. REEs (La, Y, Ce, and Nd) stayed in soluble form in the range of pH 0 – 4 (see Figure S6). Uysal [70] explained the formation of Sb depending on pH value in detail, but the hydrolysis mechanism of Sb is not fully understood. Considering previous studies, a series of experiments were conducted. The results obtained from the hydrolysis test are listed in Table 9. Sb ions from the PLS were hydrolyzed with a precipitation rate of 47.78 – 99.38 % depending on the experimental conditions, while the precipitation rate of Fe from the PLS was in a range of 2.14 % – 98.83 %.

Different options can be selected in the Taguchi approach to evaluate the experimental results. These are: “larger to better”, “smaller is better, and “nominal is the best”. Herein, it was aimed at increasing the precipitation rate of Sb while minimizing the precipitation rate of Fe from the PLS. Therefore, the “larger-to-better” option was selected to evaluate the precipitation rate of Sb, and the “smaller-is-better” option was used for the precipitation of Fe. Fig. 17 shows the values of S/N ratio calculated based on S/N analysis. The effects of hydrolysis conditions can be easily determined from these S/N graphs.

As such, the influences of precipitation conditions (from the highest to the lowest effect) on the precipitation rate of Sb was ordered as follows: pH>stirring speed > alkali type > reaction temperature. To obtain Sb-precipitate with high recoveries, the hydrolysis test should be carried out using NaOH in a temperature of 70 °C at the solution pH of 3 in the PLS that had been stirred at 100 rpm. The S/N values for the precipitation of Fe indicate that an increase in the solution pH up to 3 with the addition of NaOH resulted in the precipitation of Fe together with Sb (Fig. 18).

The ANOVA analysis given in Table S3 showed that the solution pH and stirring speed strongly affect the precipitation rate of Sb. The R-squared value for the model was 85.39 %. The effect of alkaline types and temperature was negligible for Sb precipitation. However, the precipitation rate of Fe was highly dependent on all production parameters. The R-squared value for the model was 91.40 %.

The precipitates were washed with water or alkaline and dried at 105 °C for 2 h in an oven. The crystallographic properties of the selected precipitates were imaged by SEM, as shown in Fig. 19. The obtained precipitates had amorphous structures. EDX analysis proved the precipitation of Fe together with Sb in the precipitate. The precipitate contained in range of 13.13 % – 21.45 % Fe, depending on the precipitation conditions. For example, the precipitate (obtained under the Exp. No:3 conditions) mainly comprised 55.05 % Sb, 23.51 % O, and 21.45 % Fe.

It was aimed at decreasing the Fe content in the precipitate. The contour diagrams show the effects of pH and stirring speed on the

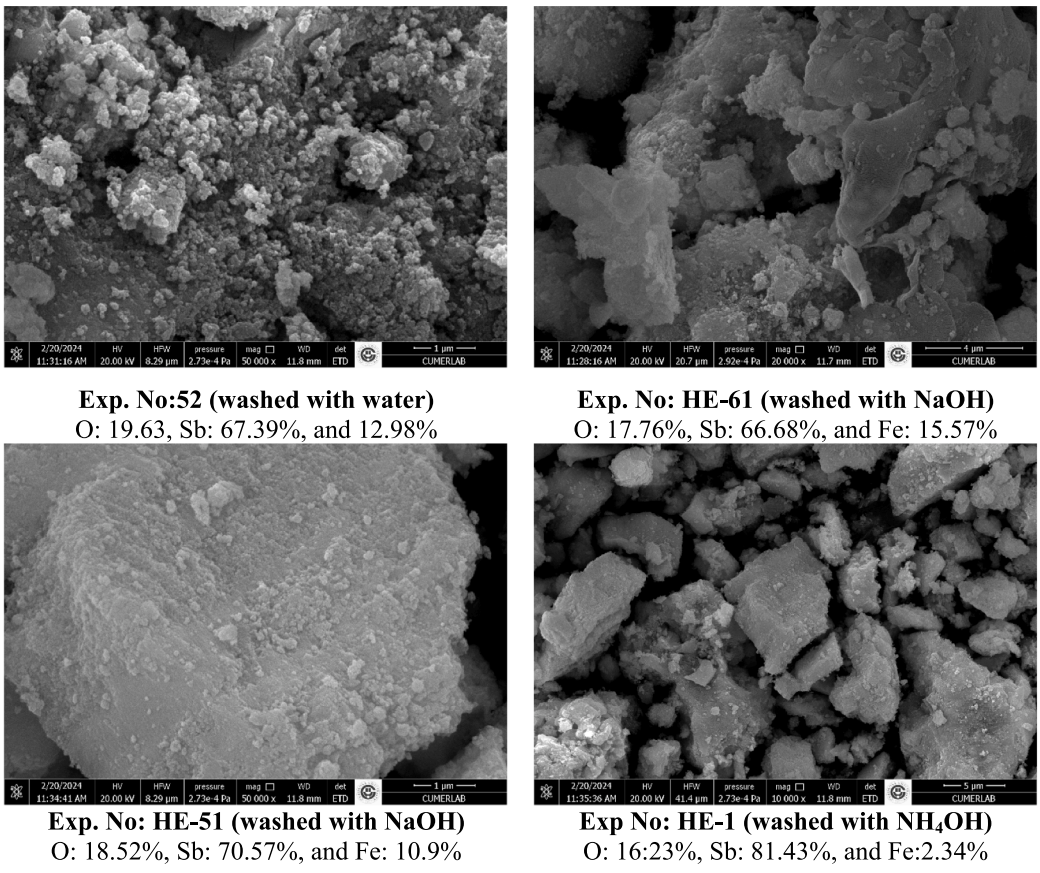

Fig. 23. SEM images of the selected precipitates obtained in the additional hydrolysis test and their chemical compositions determined by EDX after the washing procedure.

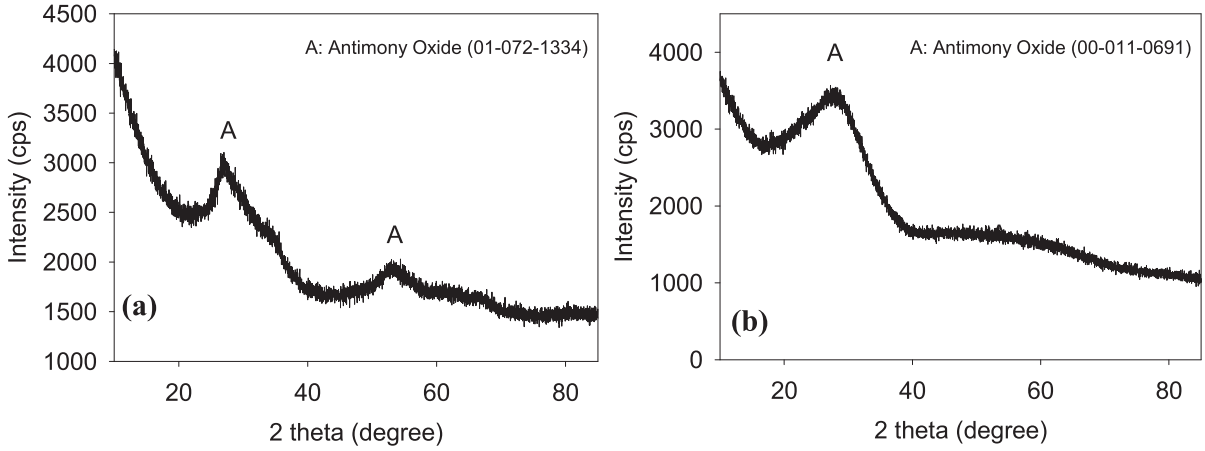

Fig. 24. XRD pattern of the selected product (a) HE-1 and (b) HE-5.

precipitation rate of Sb and Fe from the PLS, respectively (Fig. 20). The precipitation rates of Sb and Fe from the PLS increased with the increase of the pH. The contour diagrams indicate that the stirring speed strongly influenced the precipitation rate of Sb and Fe. During the hydrolysis test, if the PLS was stirred at higher speeds the precipitation rate for both elements started to decrease. For example, the precipitation rates of Sb and Fe were found to be around 75 % and 20 % when the solution pH was 1.7 and the stirring speed was $<$ 150 rpm. It was decided to conduct additional hydrolysis tests at a solution pH of $\leq$ 1.50.

The precipitation rate of Sb was higher than that of 80 % at a solution pH of 1.0 under the Exp. No HE-1. However, a decrease in the precipitation rate of Sb was determined when the solution pH reached 1.25 or 1.00 using NaOH (HE-5 and HE-6). Furthermore, there were no precipitates with the addition of NH_4OH (Fig. 21a). Depending on conditions, the precipitates with different colors were obtained (Fig. 21b).

It was understood from the SEM analyses given in Fig. 22 that the washing procedure must be carried out when the hydrolysis test ended up. The EDX analysis was performed on the selected precipitates. The presence of Cl in the precipitate was observed in a range of 42.97 % – 65.02 %, which was easily removed by the washing process. Fig. 23 shows the SEM images of the washed precipitates that contain no

chlorine ions.

The precipitate, which was obtained under Exp No HE-1 conditions, contained 81.43 % Sb, 16.23 % O, and 2.34 % Fe. Considering all results, it was decided to use NH_4OH rather than NaOH to prepare Sb-precipitate with desired purities as the precipitation rate of Fe was higher when NaOH was used. The precipitates were identified as antimony oxide minerals in XRD analysis. However, the XRD patterns of the selected products given in Fig. 24 indicated that the amorphization of the product was high due to the low peak intensities.

4. Conclusions

In this study, it was aimed to investigate the recovery of Sb from a smelter slag (4.13 % Sb) generated in a smelting furnace using HCl leaching and hydrolysis processes. The characterization of the slag was determined using various techniques, including physico-chemical properties (pH, moisture, odor, organic matter content, inorganic content), TCLP, and SPLP. Preliminary leaching tests were carried out to determine the parameters and their levels for subsequent stages. Considering these results, it was determined that Sb (III) species may form chloro-complexes and its solubility increases within increasing Cl^- ions activity. The best conditions for the leaching process were determined as follows: a HCl concentration of 8 M, a solid-to-liquid ratio of 1/10, a stirring speed of 300 rpm, tartaric acid amount of 1 g/L, a reaction temperature of 75 °C and a reaction time of 180 min. The leaching mechanism of the slag was evaluated by different shrinking core models. The Ea was calculated to be 46.75 kJ/mol, which indicates that the leaching of Sb from the slag was governed by the chemically controlled mechanism. The use of tartaric acid had a significant influence on the leaching of La from the slag. An increase in the amount of tartaric acid makes the extraction of La with high rates in shorter times. Under the best leaching conditions, the extraction rate of Sb from the slag was determined to be 91.19 % while the extraction rate of La was approximately 97 %. The extraction rates of other REEs (Y, Ce, Nd) were measured to be $\leq$ 50 %. The hydrolysis tests were conducted based on the Taguchi approach (L32, 2^1 4^3). The presence of Fe in the PLS created pollution problems in the precipitate obtained after the hydrolysis. Sb ions from the PLS were hydrolyzed with a precipitation rate of 47.78 – 99.38 % depending on the experimental conditions, while the precipitation rate of Fe from the PLS was in a range of 2.14 % – 98.83 %. The validation of these models was proved by the ANOVA analysis. Additional hydrolysis tests were carried out at pH$\leq$1.5. Depending on the pH, the precipitates with different colours were obtained due to the precipitation of Fe together with Sb. NH_4OH was suggested to use in the hydrolysis test to obtain precipitate with higher purities. The final product was mainly composed of 47.13 % Sb, 10.23 % O, and 2.51 % Fe. The product was identified as antimony oxide (Sb_2O_3). The recovery of precious metals such as Au and Ag from the slag will be investigated in the near future.

CRediT authorship contribution statement

Ahmedaljaali Ibrahim Idrees Ibrahim: Investigation, Writing – original draft. **Muhammed Aboelgamel:** Investigation. **Kartal Kaan Soylu:** Investigation. **Soner Top:** Investigation, Conceptualization, Methodology, Writing – review & editing. **Sait Kursunoglu:** Investigation, Conceptualization, Methodology, Writing – review & editing. **Mahmut Altiner:** Investigation, Conceptualization, Methodology, Funding acquisition, Project administration, Resources, Supervision, Writing – original draft, Writing – review & editing.

Declaration of competing interest

The authors declare that they have no known competing financial interests or personal relationships that could have appeared to influence the work reported in this paper.

Data availability

Data will be made available on request.

Acknowledgements

This study was supported by the Scientific and Technological Research Council of Turkey (TUBITAK) under Grant Number 123M062. The author thanks TUBITAK for their support. Also, the author would like to thank Cukurova University Research Fund for financial support (FYL-2022-15229). In addition, the authors would like to thank Dr. Burcu Selen CAGLAYAN for her help to evaluate XPS analysis.

Appendix A. Supplementary material

Supplementary data to this article can be found online at https://doi.org/10.1016/j.seppur.2024.129355.

References

[1] M. Miller, Antimony 1973 (1973) 45–50.
[2] R. Boyle, I. Jonasson, The geochemistry of antimony and its use as an indicator element in geochemical prospecting, J. Geochem. Explor. 20 (1984) 223–302.
[3] X. Zhang, S. Friedrich, B. Friedrich, Separation behavior of arsenic and lead from antimony during vacuum distillation and zone refining, J. Mater. Res. Technol. 9 (2020) 4386–4398.
[4] C. Anderson, Hydrometallurgically treating antimony-bearing industrial wastes, JOzM 53 (2001) 18–20.
[5] S. Mostashari, S. Baie, Thermogravimetry studies of cotton fabric's flame-retardancy by means of synergism of lithium bromide and antimony trioxide, J. Therm. Anal. Calorim. 94 (2008) 97–101.
[6] A. Beutl, D. Henriques, V. Motalov, D. Cupid, T. Markus, H. Flandorfer, A thermodynamic investigation of the Li–Sb system, J. Therm. Anal. Calorim. 131 (2018) 2673–2686.
[7] E. Öztürk, S. Aksöz, Y. Altıntas, K. Keşlioğlu, N. Maraşlı, Experimental measurements of some thermophysical properties of solid CdSb intermetallic in the Sn–Cd–Sb ternary alloy, J. Therm. Anal. Calorim. 126 (2016) 1059–1065.
[8] A.S. Hassanien, I.M. El Radaf, Effect of fluorine doping on the structural, optical, and electrical properties of spray deposited Sb_2O_3 thin films, Mater. Sci. Semicond. Process. 160 (2023) 107405.
[9] K.H. Abass, N.H. Obaid, A.M. Kadim, K.A. Mohammed, R.S. Zabiba, M.A. Alkhafaji, S. Sharma, A. Kumar, M. Abbas, Novel preparation of Sb_2O_3:Ag/Si solar cell fabricated utilising thermal evaporation method: studies on structural, morphology microstructural, topographic imaging, optical, and electrical properties for photovoltaic cell based electronic device applications, Appl. Phys. A 130 (2024) 81.
[10] A. Government, Critical minerals at Geoscience Australia, 2024. https://www.ga.gov.au/scientific-topics/minerals/critical-minerals.
[11] E. Commission, 2023 of critical raw materials for the EU, 2023. https://op.europa.eu/en/publication-detail/-/publication/57318397-fdd4-11ed-a05c-01aa75ed71a1.
[12] D.-P. Zhong, L. Li, C. Tan, Recovery of antimony from antimony-bearing dusts through reduction roasting process under CO—CO_2 mixture gas atmosphere after firstly oxidation roasted, J. Cent. South Univ. 25 (2018) 1904–1913.
[13] C. Anderson, Antimony production and commodites, in: R. C (Ed.) Mineral Processing and Extractive Metallurgy Handbook, SME, USA: Society for Mining, Metallurgy and Exploration, 2019. 431-442.
[14] X. Guo, K. Wang, M. He, Z. Liu, H. Yang, S. Li, Antimony smelting process generating solid wastes and dust: characterization and leaching behaviors, J. Environ. Sci. (China) 26 (2014) 1549–1556.
[15] F. Binz, B. Friedrich, Recovery of antimony trioxide flame retardants from lead refining residues by slag conditioning and fuming, Chem. Ing. Tech. 87 (2015) 1569–1579.
[16] T. Palden, L. Machiels, M. Regadío, K. Binnemans, Antimony recovery from lead-rich dross of lead smelter and conversion into antimony oxide chloride ($Sb_4O_5C_{l2}$), ACS Sustain. Chem. Eng. 9 (2021) 5074–5084.
[17] C. Tan, L. Li, K. Li, D. Zhong, Separation of As from high As-Sb dust using Fe_2O_3 as a fixative under O2–N2 atmosphere, Sep. Purif. Technol. 194 (2018) 81–88.
[18] J. Han, Z. Ou, W. Liu, F. Jiao, W. Qin, Recovery of antimony and bismuth from tin anode slime after soda roasting–alkaline leaching, Sep. Purif. Technol. 242 (2020) 116789.
[19] J. Han, C. Liang, W. Liu, W. Qin, F. Jiao, W. Li, Pretreatment of tin anode slime using alkaline pressure oxidative leaching, Sep. Purif. Technol. 174 (2017) 389–395.
[20] C. Anderson, The metallurgy of antimony, Geochemistry 72 (2012) 3–8.
[21] T. Zhao, The metallurgy of antimony, Central South University of Technology Press Changsha, China, (1988). 731 pages.
[22] G. Alev, Recovery of antimony generated in waste lead-acid battery, MSc Thesis, Istanbul Technical University, Dept. of Metallurgy and Materials Engineering, (2019). 81 pages.

[23] W. Liu, T. Yang, D. Zhang, L. Chen, Y. Liu, A new pyrometallurgical process for producing antimony white from by-product of lead smelting, JOM 66 (2014) 1694–1700.
[24] T. Gutknecht, C. Forsgren, B.-M. Steenari, Investigations into high temperature separation of antimony from metal oxide varistors, J. Clean. Prod. 162 (2017) 474–483.
[25] T. Karlsson, C. Forsgren, B.-M. Steenari, Recovery of antimony: a laboratory study on the thermal decomposition and carbothermal reduction of Sb (III), Bi (III), Zn (II) oxides, and antimony compounds from metal oxide varistors, J. Sustain. Metall. 4 (2018) 194–204.
[26] B. Zhang, Q. Li, W. Shen, X. Min, Recovery of bismuth and antimony metals from pressure-leaching slag, Rare Met. 31 (2012) 102–106.
[27] S.A. Awe, J.-E. Sundkvist, N.-J. Bolin, Å. Sandström, Process flowsheet development for recovering antimony from Sb-bearing copper concentrates, Miner. Eng. 49 (2013) 45–53.
[28] S.A. Awe, Å. Sandström, Selective leaching of arsenic and antimony from a tetrahedrite rich complex sulphide concentrate using alkaline sulphide solution, Miner. Eng. 23 (2010) 1227–1236.
[29] E. Díaz, J.A. Maldonado Calvo, J.M. Gallardo, A. Paúl, Extraction of antimony from a hydrochloric acid side stream of copper electro-refining by hydrolysis, Hydrometall. 219 (2023) 106076.
[30] R.L. Zhang, X.F. Zhang, S.Z. Tang, A.D. Huang, Ultrasound-assisted HCl-NaCl leaching of lead-rich and antimony-rich oxidizing slag, Ultrason Sonochem 27 (2015) 187–191.
[31] D. Dupont, S. Arnout, P.T. Jones, K. Binnemans, Antimony recovery from end-of-life products and industrial process residues: a critical review, Journal of Sustainable Metallurgy 2 (2016) 79–103.
[32] S. Dembele, A. Akcil, S. Panda, Technological trends, emerging applications and metallurgical strategies in antimony recovery from stibnite, Miner. Eng. 175 (2022) 107304.
[33] H. Ling, A. Malfliet, B. Blanpain, M. Guo, A review of the technologies for antimony recovery from refractory ores and metallurgical residues, Miner. Process. Extr. Metall. Rev. 45 (2022) 200–224.
[34] T. Yang, S. Rao, W. Liu, D. Zhang, L. Chen, A selective process for extracting antimony from refractory gold ore, Hydrometall. 169 (2017) 571–575.
[35] L. Ye, Z. Ouyang, Y. Chen, Y. Chen, Ferric chloride leaching of antimony from stibnite, Hydrometall. 186 (2019) 210–217.
[36] X. Hu, X. Guo, M. He, S. Li, pH-dependent release characteristics of antimony and arsenic from typical antimony-bearing ores, J Environ Sci (china) 44 (2016) 171–179.
[37] C. Rodríguez-Rodríguez, F. Nava-Alonso, A. Uribe-Salas, J. Viñals, Pyrargyrite (Ag_3SbS_3): silver and antimony dissolution by ozone oxidation in acid media, Hydrometall. 164 (2016) 15–23.
[38] Q. Tian, H. Wang, Y. Xin, D. Li, X. Guo, Ozonation leaching of a complex sulfidic antimony ore in hydrochloric acid solution, Hydrometall. 159 (2016) 126–131.
[39] I.D. Groenewald, The polarographic determination of lead in antimony sulphide flotation concentrates, Analyst 89 (1964) 140–141.
[40] I.R.Z.S.B. Moldan, The determination of silver in sulphide minerals by absorption spectrophotometry, Analytiac Chim. Acta 37 (1966) 27–32.
[41] Y. Zhang, C. Wang, B. Ma, X. Jie, P. Xing, Extracting antimony from high arsenic and gold-containing stibnite ore using slurry electrolysis, Hydrometall. 186 (2019) 284–291.
[42] H.-Z. Cao, J.-Z. Chen, H.-J. Yuan, G.-Q. Zheng, Preparation of pure SbCl3 from lead anode slime bearing high antimony and low silver, Trans. Nonferrous Met. Soc. Chin. 20 (2010) 2397–2403.
[43] M. Sudová, M. Sisol, M. Kanuchova, M. Marcin, J. Kurty, Environmentally friendly leaching of antimony from mining residues using deep eutectic solvents: optimization and sustainable extraction strategies, Processes 12 (3) (2024) 555.
[44] L. Ye, Z. Ouyang, Y. Chen, H. Wang, L. Xiao, S. Liu, Selective separation of antimony from a Sb-Fe mixed solution by hydrolysis and application in the hydrometallurgical process of antimony extraction, Sep. Purif. Technol. 228 (2019) 115753.
[45] H. Hashimoto, T. Nishimura, Y. Umetsu, Hydrolysis of antimony (III)-hydrochloric acid solution at 25° C, Mater. Trans. 44 (2003) 1624–1629.
[46] Y. Hu, H. Zhang, H. Yang, Direct synthesis of Sb_2O_3 nanoparticles via hydrolysis-precipitation method, J. Alloy. Compd. 428 (2007) 327–331.
[47] L. Meng, S.-G. Zhang, D.-A. Pan, B. Li, J.-J. Tian, A.A. Volinsky, Antimony recovery from SbCl5 acid solution by hydrolysis and aging, Rare Met. 34 (2015) 436–439.
[48] H. Ling, B. Blanpain, M. Guo, A. Malfliet, Characterization of antimony-containing metallurgical residues for antimony recovery, J. Clean. Prod. 327 (2021) 129491.
[49] H. Ling, A. Malfliet, B. Blanpain, M. Guo, Selective removal of arsenic from crude antimony trioxide by leaching with nitric acid, Sep. Purif. Technol. 281 (2022) 119976.
[50] W.L. Pohl, Economic geology: principles and practice, John Wiley & Sons, 2011.
[51] S. Ubaldini, F. Veglio, P. Fornari, C. Abbruzzese, Process flow-sheet for gold and antimony recovery from stibnite, Hydrometall. 57 (2000) 187–199.
[52] U.E.P. Agency, Method 1312: Synthetic precipitation leaching procedure, Test methods for evaluating solid waste, physical/chemical methods, (1994).
[53] J.G. Speight, Reaction mechanisms in environmental engineering: analysis and prediction, Butterworth-Heinemann, 2018.
[54] K.H. Jo, K.H. Yoon, Preparation of sol-gel derived (Ba0. 2Pb0. 8) TiO3 powders, Materials research bulletin, 24 (1989) 1-9.
[55] A. Fallis, Toxicity characteristic leaching procedure, method 1311, J. Chem. Inf. Model. https://doi.org/10.1017/CBO9781107415324, 4 (1992).
[56] L. de Andrade Lima, L. Bernardez, Characterization of the lead smelter slag in Santo Amaro, Bahia, Brazil, J. Hazard. Mater. 189 (2011) 692–699.
[57] S. Nikfar, A. Parsa, N. Bahaloo-Horeh, S.M. Mousavi, Enhanced bioleaching of Cr and Ni from a chromium-rich electroplating sludge using the filtrated culture of Aspergillus niger, J. Clean. Prod. 264 (2020) 121622.
[58] A.S. Schwoeble, B.R. Strohmeier, K.L. Bunker, D.R. McAllister, J.P. Marquis Jr, J.D. Piasecki, N.M. McAllister, Application of X-ray photoelectron spectroscopy (XPS) for the surface characterization of Gunshot Residue (GSR), Microscopy Today, 19 (2011) 40-45.
[59] J. Moulder, W. Stickle, P. Sobol, K. Bomben, Handbook of X-ray Photoelectron Spectroscopy, Perkin-Elmer Corporation: Eden Prairie, MN, 1992.
[60] C.D. Wagner, NIST X-ray photoelectron spectroscopy database, NIST Standarad Reference Database 20 (2000).
[61] S. Aktaş, B.N. Çetiner, Investigation of alkaline leaching parameters on stibnite concentrate, Min. Metall. Explorat. 37 (2020) 1729–1739.
[62] L.G. Sillen, Stability constants of metal-ion complexes, Special publication, 1971.
[63] B.N. Çetiner, Extraction of antimony from its native suphide and oxide containing ores by microwave leaching, arsenic elemination and nano size antimony synthesis, in: Metallurgy and Materials Engineering, Marmara University, Istanbul, 2022, pp. 127.
[64] S. Chae, K. Yoo, C.B. Tabelin, R.D. Alorro, Hydrochloric acid leaching behaviors of copper and antimony in speiss obtained from top submerged lance furnace, Metals 10 (10) (2020) 1393.
[65] Ö. Küçükoğlu, B.N. Çetiner, M.H. Morcalı, S. Aktaş, Comparison of the antimony cementation from chloride media using various cementators, Min. Metall. Explorat. (2022) 793–804.
[66] X.-Y. Guo, Y.-T. Xin, H. Wang, Q.-H. Tian, Leaching kinetics of antimony-bearing complex sulfides ore in hydrochloric acid solution with ozone, Trans. Nonferrous Met. Soc. Chin. 27 (2017) 2073–2081.
[67] T. Havlík, Kinetics of heterogeneous reactions of leaching processes, Hydrometallurgy Principles and Applications, Woodhead Publishing Series in Metals and Surface Engineering (2008). 184-241.
[68] J.A. Brahim, S.A. Hak, B. Achiou, R. Boulif, R. Beniazza, R. Benhida, Kinetics and mechanisms of leaching of rare earth elements from secondary resources, Miner. Eng. 177 (2022) 107351.
[69] J. Liang, S. Zhang, C. Liao, L. Xiao, G. Wang, Effects of tartaric acid, citric acid and malic acid removing lanthanum from polluted soils, J. Ecol. Rural Environ. 32 (2016) 115–119.
[70] A. Uysal, Antimony recovery from various antimony solutions by cementation and process optimization, in: Dept of Metallurgical and Materials Engineering, Marmara University, 2019, pp. 56.
[71] L. Liu, Z. Hu, Y. Cui, B. Li, X. Zhou, A facile route to the fabrication of morphology-controlled Sb2O3 nanostructures, Solid State Sci. 12 (2010) 882–886.
[72] J. Han-ying, Physical chemistry of hydrometallurgy, in, Beijing: Metallurgical Industry Press, 1984.
[73] X. Du, Research on the hydrolysis equilibrium of antimony trichloride in the Sb 3 +–Cl−–H 2 O system, Trans. Nonferrous Metals Soc. China 41 (2012) 75–79.